FOREWORD

This report presents results of work performed at REMTECH's Huntsville office. The work was conducted for Marshall Space Flight Center (MSFC) in response to requirements of Contract NAS8-28115.

The NASA Technical Coordination for this study was provided by Mr. Homer Wilson and Mr. John Warmbrod of the Thermal Environment Branch of the Aero-Astrodynamics Laboratory. In addition, the authors would like to express apprecaition to Mr. R. Elkin, Mr. D. Seymour, and Dr. T. Greenwood of the Thermal Environment Branch for technical assistance relative to specific aspects of this work.

TABLE OF CONTENTS

LIST OF TABLES

LIST OF FIGURES

Section 1

INTRODUCTION

Several technical areas were encompassed in providing support for Booster thermal environment test work. These areas included cavity flow heating, rarefied flow heating and impulse operated model research and testing. Cavity flow heating problems were studied with respect to the proposed altitude control motors for the Space Shuttle. Available literature on this subject was reviewed and analytical predictive methods were summarized for use in planning testing work. Rarefied flow heating data was reviewed and correlated. The study showed the importance of considering rarefied flow conditions in launch thermal environment prediction. Impulse operated model research and testing was conducted to provide a basis for understanding and designing such models for booster thermal environment testing. During the course of this work technical reports were completed which document the various technical facits encompassed. This set of reports, Refs. 1 to 13, provides comprehensive documentation and thus a synoptic presentation method is used herein. The most salient features of the work are given in the following sections.

Section 2

CAVITY HEATING

Propulsive attitude control systems which are intermittently used during hypersonic atmospheric flight are discussed and analyzed as an open cavity flow heat transfer problem in Ref. 1. The literature which presents open cavity flow characteristics is reviewed and discussed in terms of ACS nozzle-cavity heating. A description of existing analytical models for prediction of heat transfer within cavities is given in Ref. 1 and are summarized here. All of the models presented were developed for two-dimensional laminar flow (see Fig. 1). Thus, unless three-dimensional effects within ACS nozzle cavities are found to be negligible these models will require modification to be applicable to ACS nozzle flow. Furthermore, other models for turbulent flow will be required for anticipated flight conditions.

2.1   BURGGRAF'S MODEL

Burggraf (Ref. 14) modeled the steady separated flow in two-dimensional rectangular cavities at high Reynolds numbers. The cavity flow was considered to consist of a single constant enthalpy, rotating inviscid eddy which produces a thin boundary layer along the cavity walls. The laminar momentum and energy equations were linearized and the Prandtl number assumed to be one to obtain a tractable solution. The heat transfer distribution was normalized to using Chapman's average value transferred across the dividing streamline. The expression relating the preseparation heating to the distribution within the cavity is given in Table 1.

REMTECH INCORPORATED   RTR 008-4

Burggraf also examined the limitations of his analysis with respect to the assumption of an inviscid central core. The model is no longer valid when the boundary layer thickness becomes equal to one half of the cavity width, W, for cavities with H > W. This condition is related to a critical Reynolds number given by Eq. (2) of Table 1. Thus for the theory to be applicable the local edge Reynolds number, Eq. (1) of Table 1 must be greater than the critical Reynolds number given by Eq. (2) of Table 1.

As part of the present investigation, Burggraf's model was programmed to provide a predictive method. Due to the simplicity of the heat transfer correlation, the program was used to parametrically evaluate the heat transfer distribution. The results of this parametric analysis are given in Fig. 2 for W/H values spanning the range of expected ACS nozzle cavities geometries.

2.2 HODGSON'S MODEL

Hodgson (Ref. 15) visualized cavity flow as determined by an oncoming boundary which separates and forms a shear layer which in turn produces an equivalent wedge flow down the reattachment wall. The equations corresponding to this conceptual model are given in Table 2 and are discussed below.

The effect of finite upstream boundary layer was introduced through its influence on the dividing streamline velocity, U_d, as determined from results of Denison and Baum (Ref. 16). In the present work, the theoretical curve was least squares fit for numerical computation purposes.

Cavity fluid properties are computed using an average cavity temperature, Eq. (4), and the boundary layer edge pressure. The dividing streamline

3

temperature, T_d, is computed using a modified Crocco's relationship, [Eq. (3)].

One of the significant contributions of this model is the compressibility correction given for the reattachment zone length, L, expressed in Eqs. (6) and (7). This length is used in an expression for the local velcoity along the reattachemnt wall which was develcped for incompressible flow, [Eq. (8)]. Reattachment wall heat transfer is then computed using heat transfer relations [Eqs. (9) to (13)] for a flat plate having a varying freestream velocity.

The theories of Burggraf and Hodgson provides the most easily used methods for the engineer to obtain an estimate of the heating distribution within a cavity. Several additional methods and aspects of this problem are presented and discussed in Ref. 1.

The cavity heating information given in Ref. 1 was applied to a specific problem in Ref. 2. This reference documents a study of the thermal environments for two proposed cavity regions of the External Tank. Thermal environments for the exit region cf the LOX Tank Vent Line and exit region of the Intertank Deorbit Retro were computed for two trajectory points corresponding to peak heating trajectory points. Heating rates for specific points within the cavities and near the cavities on the external surface are given in tabular form in Ref. 2.

Table 1

Burggraf: Laminar 2-D Cavity Heating Equations

	Nomenclature
1. $Re_{X_0} = \dfrac{\rho_e U_e X_0}{\mu_e}$	U_e - Boundary layer (BL) edge velocity
	ρ_e - BL edge density
	μ_e - BL edge viscosity
	X_0 - BL running length to cavity
2. $Re_{cr} = 240\left(\dfrac{X_0}{W}\right)^{4/3}\left(1 + \dfrac{H}{W}\right)$	y - Distance along cavity reattachment wall from external surface
	q_{ps}- Preseparation convective heating rate
	$q(y)$-Local heating rate
3. If $Re_{X_0} > Re_{cr}$ then	W,H- See Fig. 1

$$\frac{q(y)}{q_{ps}} = \frac{.21}{\sqrt{1 + H/W}}\left[\zeta\left(\frac{1}{2}, \frac{y}{2(W+H)}\right) - \zeta\left(\frac{1}{2}, \frac{y+W}{2(W+H)}\right)\right]$$

4. Rieman zeta function (a rational approximation)

$$\zeta\left(\frac{1}{2}, x\right) = \frac{1}{\sqrt{x}} + \sum_{n=0}^{5} a_n (x+1)^n$$

$a_0 = + 0.803323$

$a_1 = - 3.89728$

$a_2 = + 2.55002$

$a_3 = - 1.19121$

$a_4 = + 0.308284$

$a_5 = - 0.0335024$

Table 2

Hodgson: Laminar 2-D Cavity Heating Equations

1. $S^* = W/X_0$ (Flat Plate)

2. $\dfrac{U_d}{U_e} = f(S^*)$ from Fig. 5 of Denison and Baum (Ref. 16)

Least Squares Fit

$$\frac{U_d}{U_e} = a_0 + a_1 \xi + a_2 \xi^2 + a_3 \xi^3 + a_4 \xi^4 + a_5 \xi^5$$

where $\xi = \log_{10}(S^*)$

$a_0 = + .51706$

$a_1 = + .088707$

$a_2 = - .049822$

$a_3 = - .0020116$

$a_4 = + .0047757$

$a_5 = + .0006549$

3. $T_d = T_W + \left(\dfrac{U_d}{U_e}\right)\left(T_{aW} - T_W\right) - \left(\dfrac{U_d}{U_e}\right)^2 \sqrt{P_r}\left(\dfrac{U_e^2}{2C_p}\right)$

4. $T_c = .5(T_d + T_W)$

5. $Re_W = \dfrac{\rho_e U_e W}{\mu_e}$

6. $L_i = \dfrac{11.8W}{Re_W^{1/2}}$

Table 2 (Continued)

7.* $L = L_1\left\{1 + 0.447\left[(\gamma-1)/2\right] M_e^2 \Big/ \left[5.22 + 4.41\left(T_w/T_e -1\right)\right]\right\}$

8. For $y/L \leq 1$

$$\frac{v}{U_d} = 1.-.189\exp\left(-5.3\,y/L\right) -10.6\sum_{n=1}^{\infty}\frac{\exp\left[-y/L(9.87n^2 + 28.1)^{1/2}\right]}{9.87n^2 + 28.1}$$

9. For $y/L \leq 1$

$$StRe_L^{1/2} = C_1\left(\frac{v}{U_d}\right)^{C_2}\Big/\left[\int_0^{y/L}\left(\frac{v}{U_d}\right)^{C_3} d\left(\frac{y}{L}\right)\right]^{1/2}$$

where for $Pr = .7$

$C_1 = 0.418$

$C_2 = 0.435$

$C_3 = 1.87$

10. For $y/L > 1$

$v = U_d$

11. For $y/L > 1$

$StRe_L^{1/2} = C_1\Big/(y/L -A)^{1/2}$

where for $Pr = 0.7$

$A = 0.178$

12. $Re_L = \dfrac{\rho_c U_d L}{\mu_c}$

13. $q = St\rho_c v C_p (T_d - T_w)$

Nomenclature	
X_0	B.L. running length to cavity
W,H	See Fig. 1
U_e	Boundary layer (BL) edge velocity
U_d	Dividing streamline velocity
T_w	Wall temperature
P_r	Prandtl number
T_{aw}	Adiabatic wall temperature
C_p	B.L. edge heat capacity
ρ_e	B.L. edge density
μ_e	B.L. edge viscosity
T_e	B.L. edge temperature
M_e	B.L. edge Mach number
μ_c	Viscosity evaluated at T_c
y	Distance along cavity reattachment wall from the external surface
γ	Ratio of specific heats
q	Local heating rate

*The misprint which occurred in this equation in Ref. 15 was corrected by personal communications with the author.

7

Separation
Shock

Reattachment
Shock

Expansion
Fan

Mixing
Zone

U_e

δ

Dividing Streamline

Separation
Point

Reattachment
Point

H

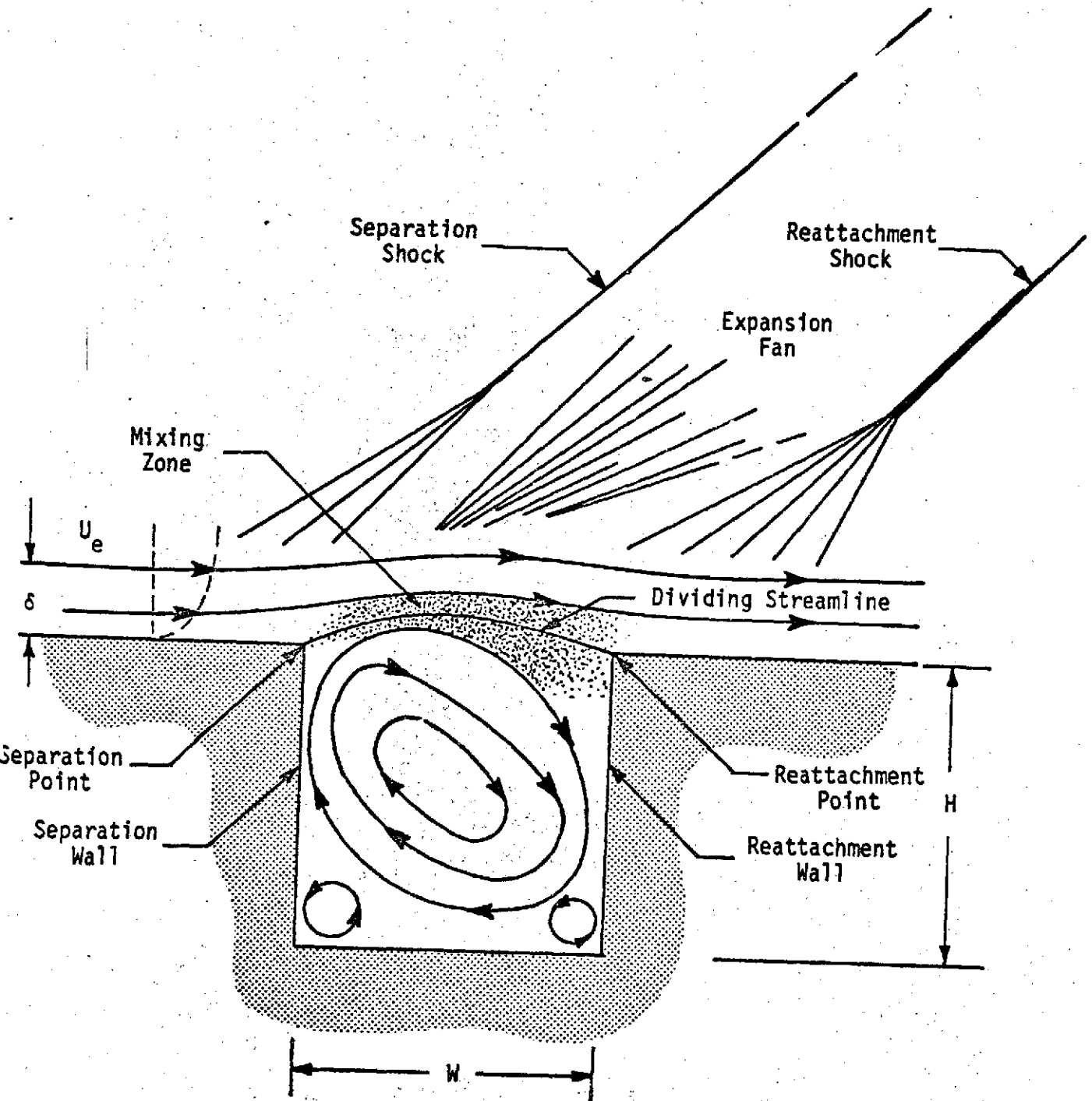Separation
Wall

Reattachment
Wall

W

Fig. 1 - Schematic of Open Cavity Flow Structure

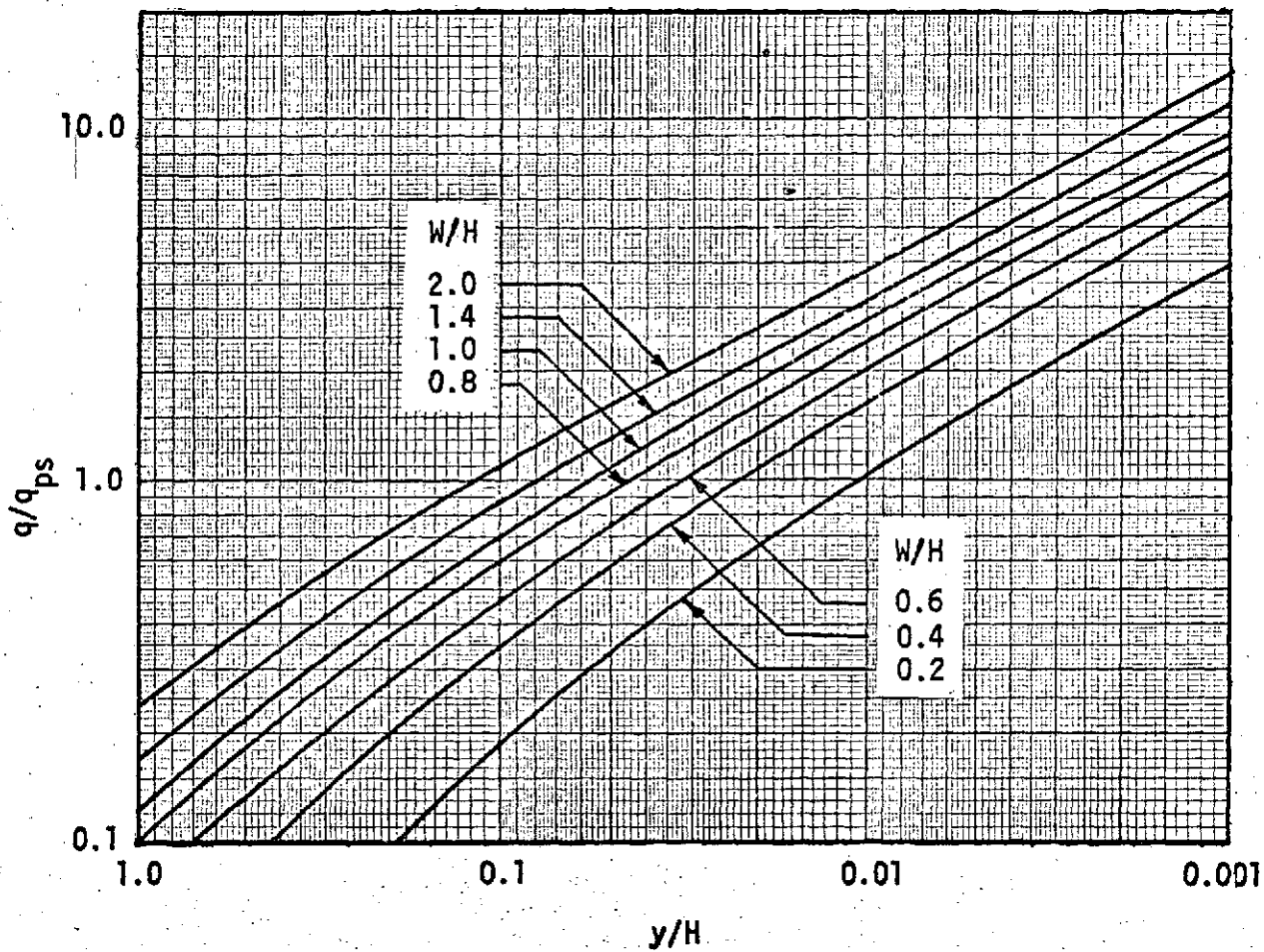q_{ps} = Preseparation Heating Rate

Fig. 2   Reattachment Wall Heating Based on Burggraf's Model

Section 3

RAREFIED FLOW HEATING

Aeroheating during hypersonic flight at rarefied conditions has become a problem of concern for Space Shuttle launch and entry. Mission requirements dictate that during ascent and entry the External Tank (ET) will spend a significant amount of time in rarefied hypersonic flight. Consequently, several reports have been prepared, Refs. 3 to 7, which detail expected flow conditions, rarefied flight predictive methods, analysis of available data and computer program documentation for methods of computing rarefied flow thermal environments. The more salient features of this work are given here.

The most significant contribution of Ref. 3 is the correlation of rarefied flow heating data in a manner which provides a rapid calculation procedure of rarefied flow heating for the design engineer. Flow regime switching criteria are given in Table 3. Relations for free molecular heating are given in Table 4. Rarefied flow heating relations and data are presented for spheres, cones, cylinders, flat plates and wedges in Tables 5 to 9 and Figs. 3 to 7. Wedge flow relations were developed subsequent to the work given in Ref. 3. In addition to the heating methods stated above, Ref. 3 provides an alternate method of scaling wind tunnel rarefied stagnation point heating to flight conditions.

The rarefied and free molecular flow heating prediction methods were programmed and incorporated into the MINIVER computer program. Ref. 6 provides documentation of the changes made and Ref. 7 provides a program listing of the entire modified computer code.

During the course of checking-out rarefied flow heating methods, it was found that a simple method was needed to compute the local recovery enthalpy.

Ref. 7 was completed in response to this need. A Newtonian and a concentric shock approach were shown to yield the same relationship for the recovery enthalpy. This relationship is given in Table 10.

In order to attempt to broaden the rarefied flow heating data base, a review of Saturn V launch data was undertaken. The basic conclusions drawn from this study (Ref. 4) are: (1) The Saturn 501 heating rate gauge output in the rarefied flow regime is of the same magnitude as the zero bias error of the respective gauges, (2) Since some of the gauge output exceeds the maximum convective heating potential, gauge output cannot be attributed to convective heating and must be due to gauge inaccuracy and/or solar radiation input and (3) The uncertainties and inconsistencies in the data precludes their use in establishing a basis for rarefied flow convective heating.

TABLE 3

FLOW REGIME CRITERIA

$$\frac{M_\infty}{\sqrt{Re_\infty}} \quad < \quad 0.05 \qquad \text{Boundary layer flow}$$

$$0.05 < \frac{M_\infty}{\sqrt{Re_\infty}} \quad < \quad 3.0 \qquad \text{Rarefied flow}$$

$$\frac{M_\infty}{\sqrt{Re_\infty}} \quad > \quad 3.0 \qquad \text{Free molecular flow}$$

TABLE 4

FREE MOLECULAR FLOW HEATING EQUATIONS*

(1) $N = \dfrac{P}{kT}$ (particles/unit volume)

(2) $S = \sqrt{\dfrac{\gamma}{2}}\ M_\infty$ (molecular speed ratio)

(3) $\psi = \dfrac{NU_\infty}{2\sqrt{\pi}\,S}$

(4) $\eta = S \sin\theta$

(5) $n = \psi\left[e^{-\eta^2} + \sqrt{\pi}\,\eta(1 + \operatorname{erf}\eta)\right]$
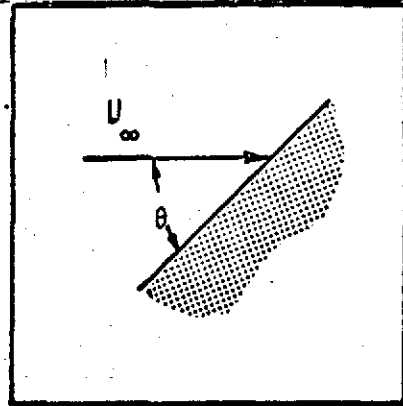
= number of molecules striking a unit area per unit time

where

$$\operatorname{erf}\eta = \frac{2}{\sqrt{\pi}}\int_0^\eta e^{-x^2}\,dx \quad \text{(error function)}$$

Rational approximation $(o \le \eta < \infty)$ from Ref. 5

$$\operatorname{erf}\eta = 1. - (a_1 t + a_2 t^2 + a_3 t^3)e^{-\eta^2} + \epsilon(\eta)$$

$$t = \frac{1}{1 + a_0 \eta}$$

$a_0 = 0.47047$

$a_1 = 0.3480242$

$a_2 = -0.0958798$

$a_3 = 0.7478556$

$\left|\epsilon(\eta)\right| \le 2.5 \times 10^{-5}$

TABLE 4 (cont.)

FREE MOLECULAR FLOW HEATING EQUATIONS

(6) $\phi = \dfrac{\psi}{2} e^{-\eta^2}$

(7) $q = \alpha \left\{ \dfrac{\gamma+1}{2(\gamma-1)} nkT_W - \left[\left(S^2 + \dfrac{\gamma}{\gamma-1} \right) n - \phi \right] kT_\infty \right\}$

= heating rate

Nomenclature

U_∞ - Freestream velocity

P - Freestream pressure

T - Freestream temperature

k - Boltzman's constant

γ - Freestream specific heat ratio

*From Oppenheim (Ref. 17)

TABLE 5

RAREFIED FLOW STAGNATION POINT HEAT TRANSFER EQUATIONS

(1) $T_r = \left(T_\delta + T_W\right)/2$

(2) $T_0 = T_\infty \left(1 + \frac{\gamma-1}{2} M_\infty^2\right)$

(3) $K^2 = \epsilon \left(\frac{\rho_\infty U_\infty R}{\mu_r}\right)\left(\frac{T_r}{T_0}\right)$

where $\epsilon = \frac{\gamma-1}{2\gamma}$

(4) Heat transfer coefficient

$$\log_{10}(C_H) = \sum_{i=0}^{2} a_i \left(\log_{10} K^2\right)^i$$

$a_0 = -0.235256$

$a_1 = -0.303095$

$a_2 = -0.0779538$

(5) Heat transfer

$q = \rho_\infty U_\infty C_H (H_\infty - H_W)$

Nomenclature

T_δ - Post normal shock temperature

T_W - Wall temperature

M_∞ - Freestream Mach number

γ - Freestream specific heat ratio

μ_r - Viscosity evaluated at T_r and P_δ

H_∞ - Total enthalpy

H_W - Wall enthalpy

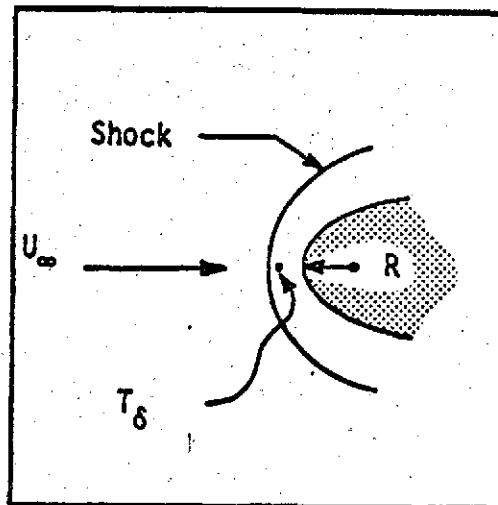ρ_∞ - Freestream density

15

TABLE 6

RAREFIED FLOW SHARP CONE
HEAT TRANSFER EQUATIONS

---

(1) $T_r = T_w + (T_\delta + T_w)/2 - T_\delta \cos^2\theta_c/3$

(2) $Re_\infty = \dfrac{\rho_\infty U_\infty x}{\mu_\infty}$

(3) $C^* = \dfrac{\mu_r\, T_\infty}{\mu_\infty\, T_r}$

(4) $\xi = \dfrac{C_H}{\sin\theta_c}\left(1 - \dfrac{T_w}{T_\delta}\right)$

(5) $\bar{X}_c = \dfrac{Re_\infty}{M_\infty^2 \gamma_\infty C^* \cos\theta_c}$

(6) Correlation Equation

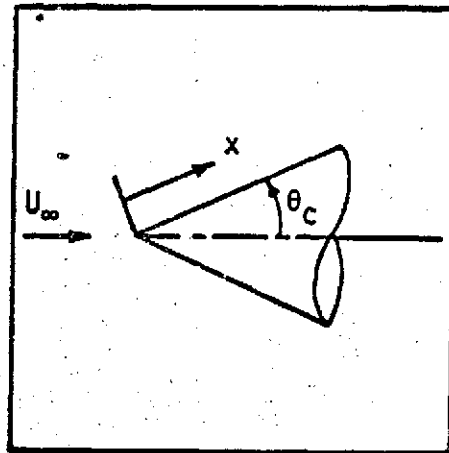$$\log_{10}(\xi) = \sum_{i=0}^{2} a_i\, (\log_{10}\bar{X}_c)^i$$

$a_0 = -0.392510$

$a_1 = -0.266308$

$a_2 = -0.0598724$

(7) Heat Transfer

$q = \rho_\infty U_\infty C_H (H_\infty - H_w)$

Nomenclature

See Table 5

TABLE 7

RAREFIED FLOW SHARP FLAT PLATE
HEAT TRANSFER EQUATIONS*

(1) $T_0 = T_\infty \left(1 + \frac{\gamma-1}{2} M_\infty^2\right)$

(2) $Re_\infty = \frac{\rho_\infty U_\infty X}{\mu_\infty}$

(3) $C_* = \frac{\mu_W T_\infty}{\mu_\infty T_W}$

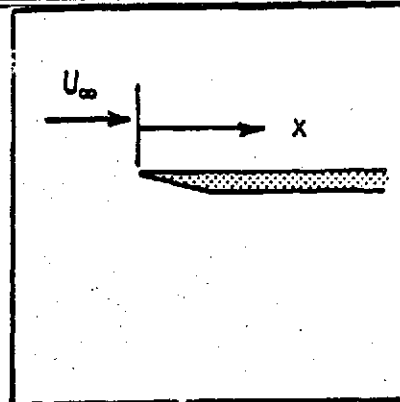(4) $\beta = (T_W/T_0)^{1/2} M_\infty^2 C_*/Re_\infty$

(5) $C_{H_{si}} = (0.368 T_W/T_0 + 0.0684)\left[M_\infty(C_*/Re_\infty)^{1/2}\right]^{3/2}$

(6) $\dfrac{C_H}{C_{H_{si}}} = \dfrac{1}{2}\left[1 - \tanh(0.91 \log_{10}\beta + 1.10)\right]$

for $\beta < 0.1$

(7) Heat Transfer

$q = \rho_\infty U_\infty C_H (H_\infty - H_W)$

Nomenclature
See Table 5

*From Shorenstein and Probstein (Ref. 18)

TABLE 8

RAREFIED FLOW YAWED CYLINDER
STAGNATION LINE HEAT TRANSFER EQUATIONS

(1) $T_r = \frac{1}{2} (T_W + T_\delta \cos^2\Lambda)$

Nomenclature

See Table 5

(2) $Re_\infty = \dfrac{\rho_\infty U_\infty R}{\mu_\infty}$

(3) $C_* = \dfrac{\mu_r \, T_\infty}{\mu_\infty \, T_r}$

(4) $\tilde{K}_\Lambda^2 = \dfrac{Re_\infty}{\gamma_\infty M_\infty^2 C_* \cos\Lambda}$

(5) $\xi = C_H / \cos\Lambda$

(6) Heat Transfer Correlation

$$\log_{10} \xi = \sum_{i=0}^{2} a_i (\log_{10}\tilde{K}_\Lambda^2)^i$$

$a_0 = -0.377656$

$a_1 = -0.368580$

$a_2 = -0.0461064$

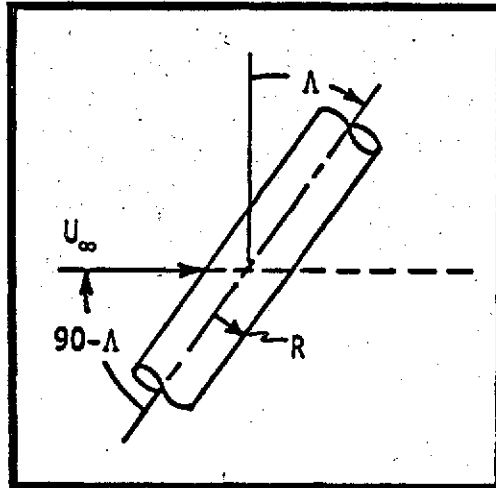(7) Heat Transfer

$q = \rho_\infty U_\infty C_H (H_\infty - H_W)$

TABLE 9

RAREFIED WEDGE FLOW HEAT TRANSFER
EQUATIONS

(1) $T_r = T_\delta/6 + T_w/2$

(2) $C_* = \dfrac{\mu_r T_\infty}{\mu_\infty T_r}$

(3) $R_{e\infty,x} = \dfrac{\rho_\infty U_\infty X}{\mu_\infty}$

(4) $K_w^2 = \dfrac{R_{e\infty,x}}{\gamma_\infty M_\infty^2 C_* \cos\theta}$

(5) $\xi = C_H/\cos\theta$

<u>Nomenclature</u>

T_δ - Post Normal Shock Temperature

T_w - Wall temperature

T_∞ - Freestream temperature

X - Surface length

U_∞ - Freestream velocity

μ_∞ - Freestream viscosity

ρ_∞ - Freestream density

γ_∞ - Freestream specific heat ratio

M_∞ - Freestream Mach no.

H_∞ - Freestream total enthalpy

H_w - Wall enthalpy

(6) Heat Transfer correlation ($\theta > 10°$)

$$\log_{10} \xi = \sum_{i=0}^{2} a_i (\log_{10} K_w^2)^i$$

$a_0 = -0.370778$

$a_1 = -0.388606$

$a_2 = -0.108383$

(7) Heat transfer

$q = \rho_\infty U_\infty C_H (H_\infty - H_w)$

TABLE 10

A SIMPLE RECOVERY ENTHALPY RELATION
FOR HYPERSONIC FLIGHT

$$H_r = h_\infty + (\sin^2\theta + r\cos^2\theta)\, U_\infty^2/2gJ$$

Nomenclature

H_r - Recovery enthalpy

h_∞ - Freestream static enthalpy

r - Recovery Factor $= P_r^{\frac{1}{2}}$ (Laminar)

$\qquad\qquad\qquad\qquad = P_r^{\frac{1}{3}}$ (Turbulent)

P_r - Prandtl number

U_∞ - Freestream velocity

g - Gravitational constant

J - Mechanical equivalent of work
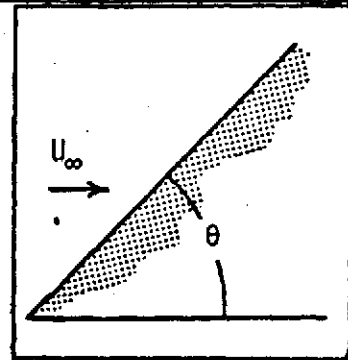
21
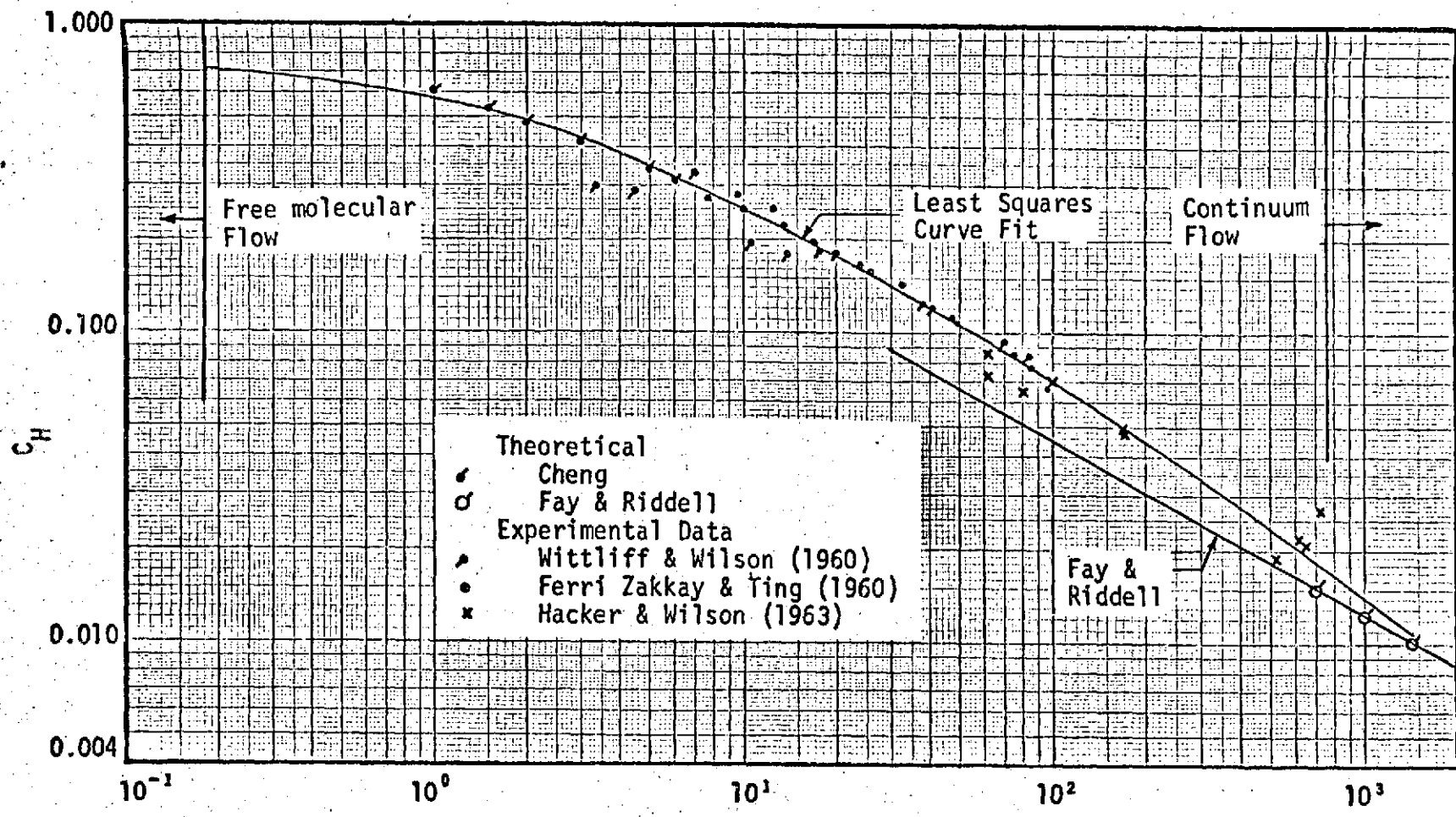
$$K^2 = \left(\frac{\gamma-1}{2\gamma}\right)_{\infty}\left(\frac{\rho_{\infty} U_{\infty} R}{\mu_r}\right)\left(\frac{T_r}{T_0}\right)$$

Fig. 3 Stagnation Point Heat Transfer Coefficient for Low Reynolds Number Flow

Fig. 4 Sharp Cone Heat Transfer Data

Continuum

Free Molecular

$$\frac{M_\infty^3 \, C_H}{\bar{X}_f^{3/2}} \times \frac{(0.768)^{1/2}}{(0.664 + 1.73 T_w/T_0)^{1/2}}$$

Exact Strong Interaction Limit

Shorenstein and Probstein (1968)

Vida & Bartz (1968) Air Shock Tunnel Experiments
$M_\infty = 19\text{-}22$

$$\bar{X}_f = M_\infty^3 \sqrt{\frac{C_*}{Re_{X_\infty}}}$$

$$C_* = \frac{\mu_*}{\mu_\infty} \frac{T_\infty}{T_*}$$

Free Molecular Flow Limit
$M_\infty = 20$, $\alpha = 1.0$

$\bar{X}_f / M_\infty^2$

Fig. 5 Comparison of Flat Plate Analyses and Experimental Heat Transfer Data

Fig. 6 Stagnation Line Heat Transfer to Yawed Cylinders

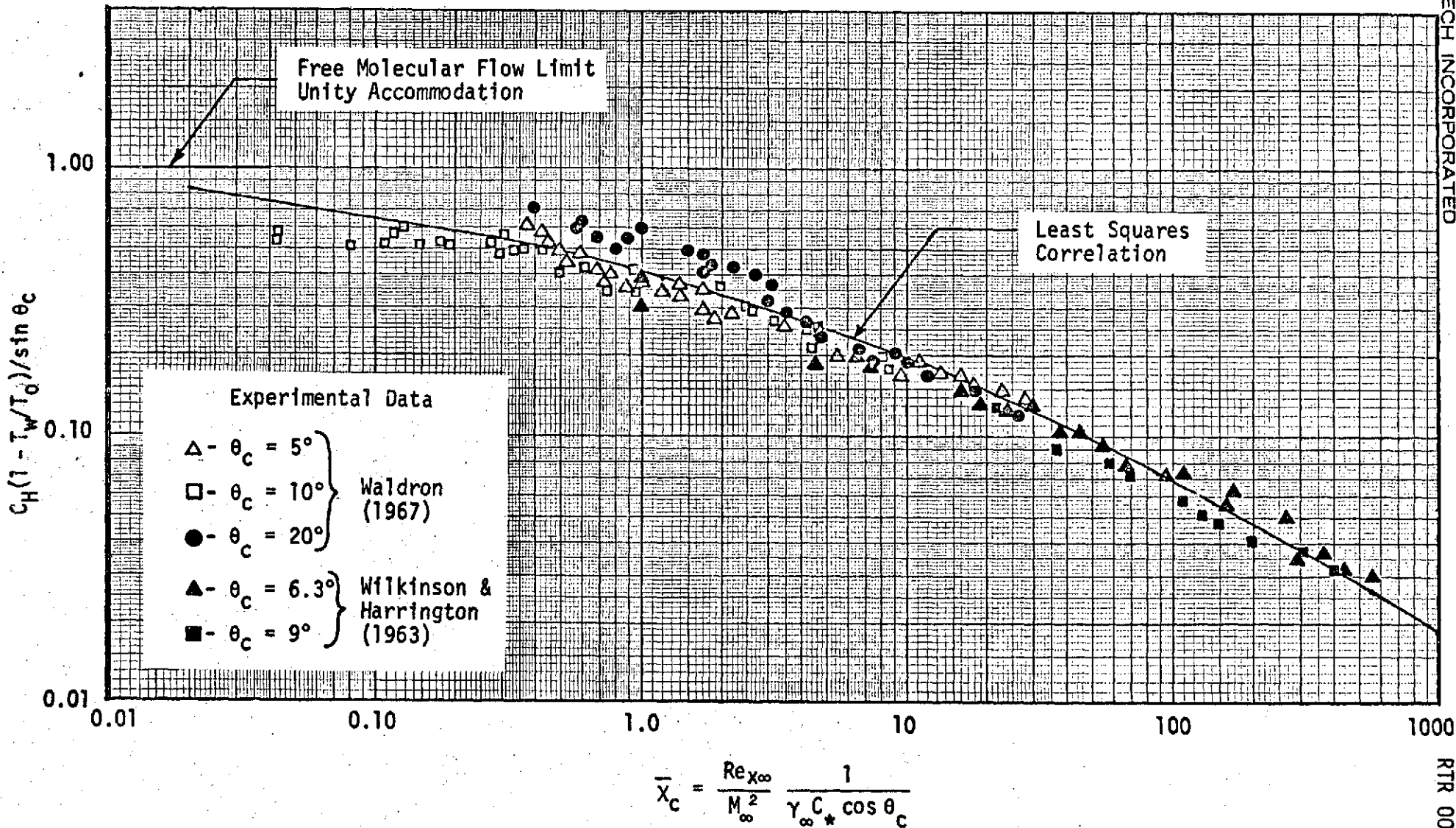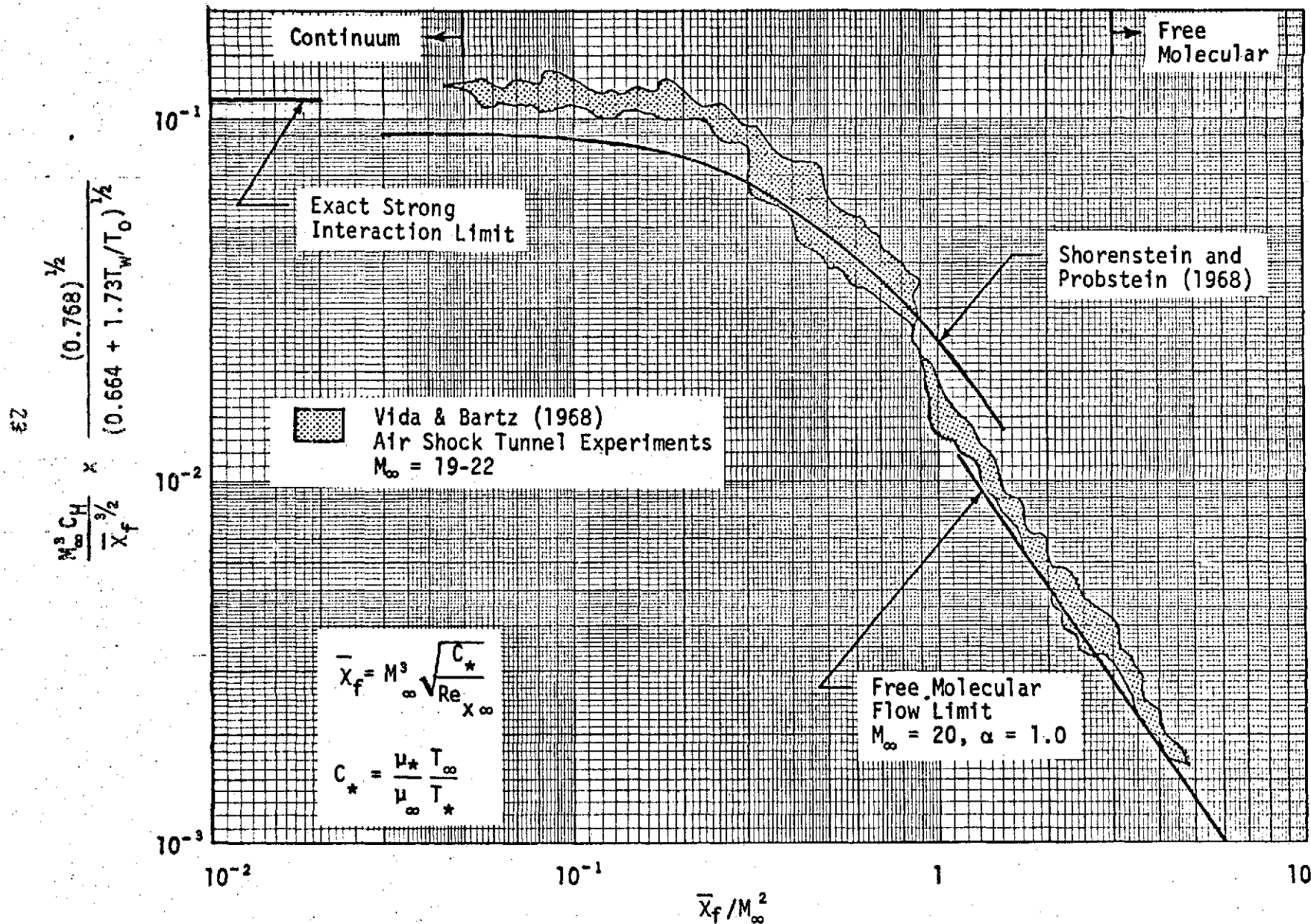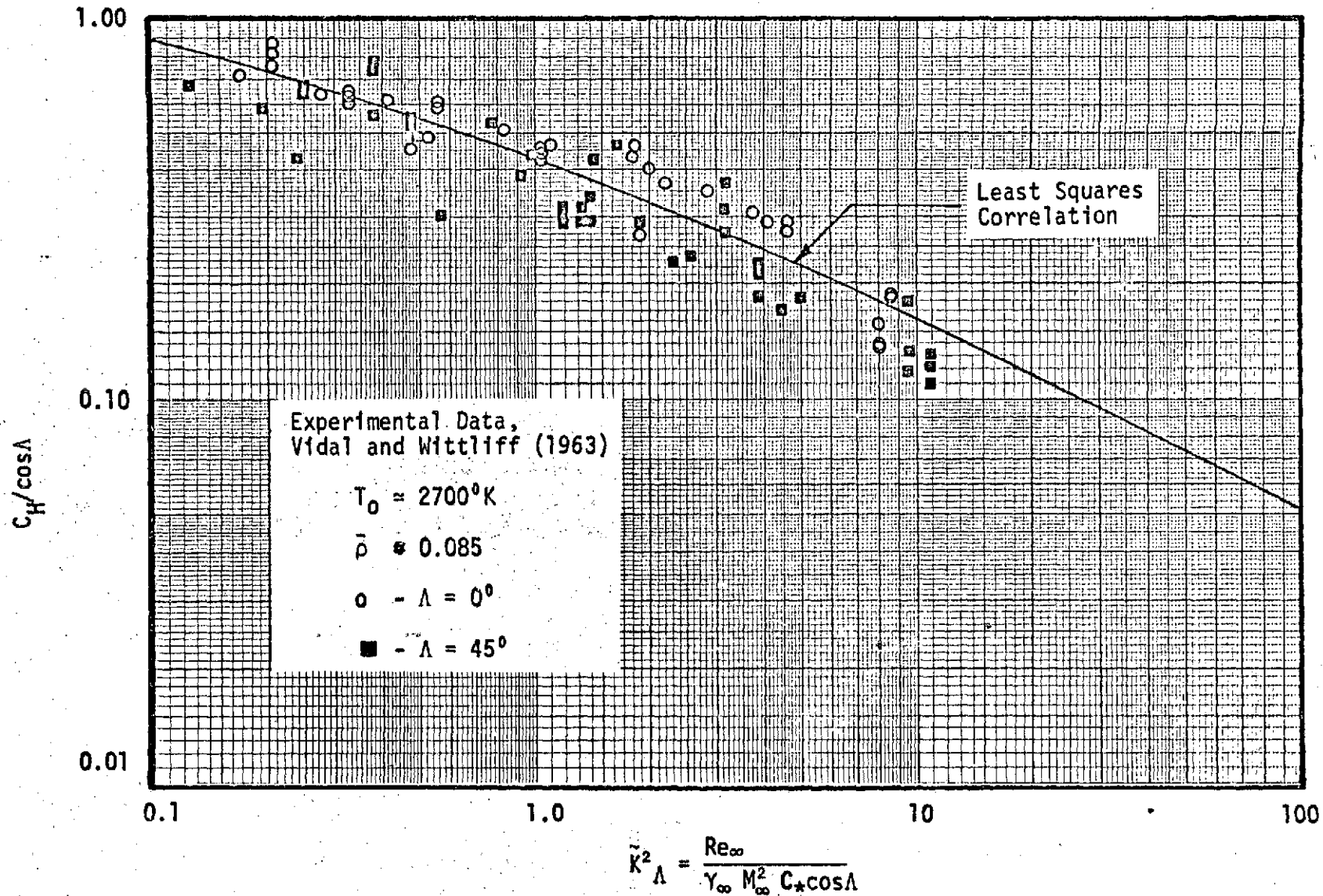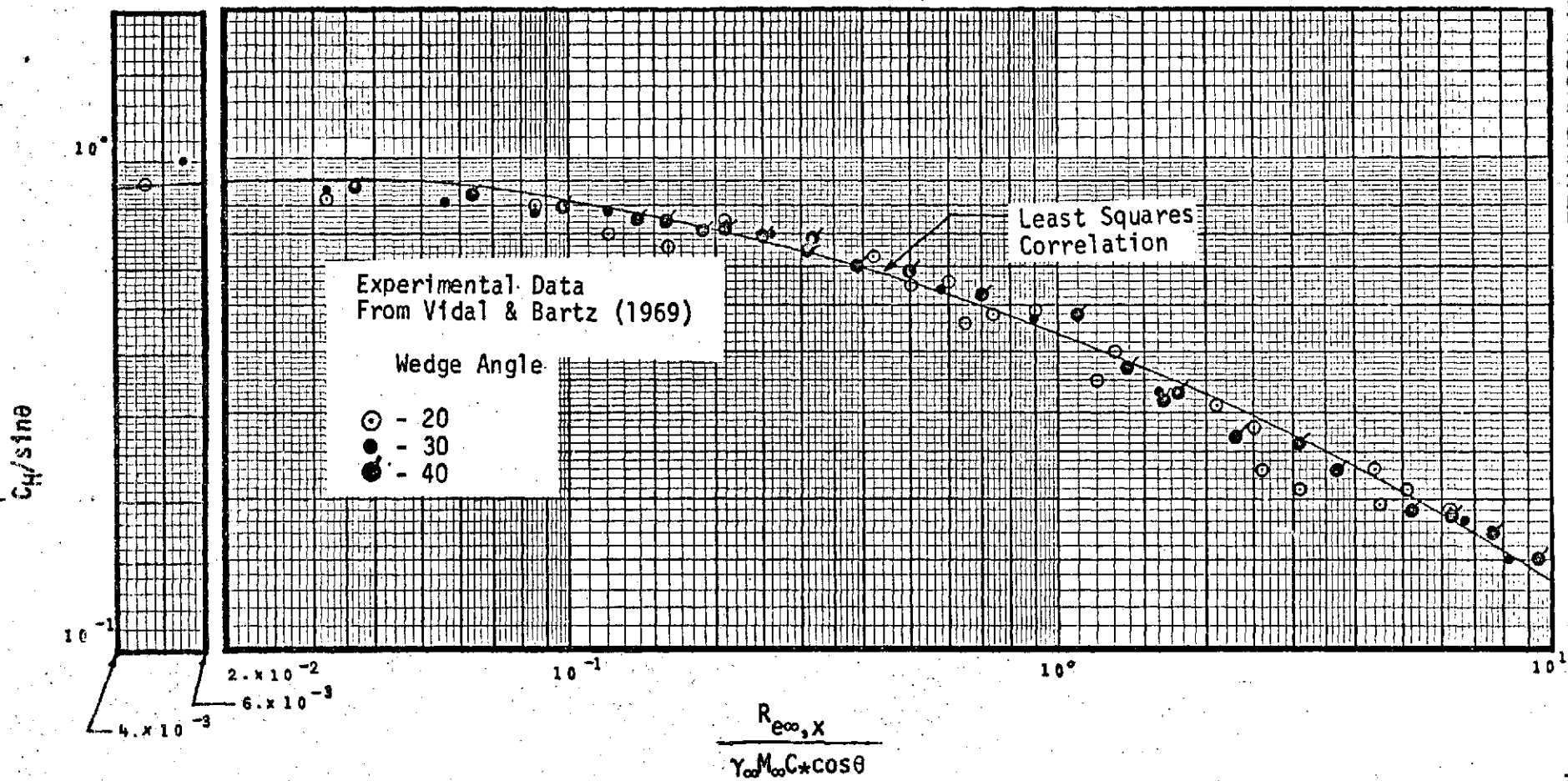Fig. 7 Low Density Wedge Flow Heat Transfer Data

Section 4

IMPULSE MODEL RESEARCH

The objective of this work was to develop a sound understanding of Impulse Base Flow Facility (IBFF) model and tank wave dynamics from which future designs could be derived. To accomplish this objective, several work items were completed. The performance of five IBFF model configurations were monitored and analyzed as they were used for other test programs (Ref. 8). Theoretical steady state H_2-O_2 combustor properties were calculated and presented in graphical form for design and/or analysis work by Ref. 11. A pretest plan (Refs. 9 and 10) was developed to obtain parametric experimental data for design of impulse operated models and blast wave tank dynamics. The test was conducted and the data analyzed and presented in Refs. 12 and 13.

4.1 IBFF DATA MONITORING

Facility model data was taken during routine testing operation of the IBFF. One hundred and twenty two (122) runs were made in which the combustor pressure, initial combustor pressure rise rate, and type of combustion were recorded. This data was taken using two injectors and two nozzle configurations with which nozzle diaphragms of various thicknesses were used.

From the data analyzed in Ref. 8 the following conclusions were drawn: Ignition Characteristics:

- Ignition resulting in hot flows were experienced in all runs using the equivalent engine with a diaphragm and a pin hole.

- It follows from the above conclusion that a glow plug is not necessary to obtain repeatable ignition of H_2 - O_2 in some configurations.

- No correlation of pin hole size or diaphragm thickness with ignition behavior was found.

- Not using a nozzle diaphragm reduces ignition reliability

- Insufficient data was available to quantitatively establish the difference between ignition characteristics of the large and small volume injectors in the equivalent engine.

- The two engine geometry exhibited poor ignition reliability. This configuration has a larger combustor volume due to the two nozzle entrance ports.

- The two engine configuration is the only configuration studied which has produced an overpressure combustor pressure response.

- The timing between H_2 and O_2 arriving at the combustor may effect the percent hot flows obtained.

Performance Characteristics

- The chamber pressure for hot flows is repeatable to within at most $\pm$ 12% of the average chamber pressure for a given geometry.

- Injector geometry and/or volume can significantly change the measured steady state chamber pressure.

- The average chamber pressure for initial overpressure runs is statistically indistinguishable from the average chamber pressure for nominal hot flow runs.

- The initial cold flow chamber pressure rise rate can be statistically distinguished from hot flow chamber pressure rise rates.

- The hot flow initial chamber pressure rise rate is statistically the same for a 0.005 in. thick nozzle diaphragm as those runs without a diaphragm.

- Runs which exhibit initial overpressure characteristic also exhibit the largest scatter in the measured steady state chamber pressure (i.e. $\pm$ 28.5% from the mean).

4.2 CHAMBER PROPERTIES OF GASEOUS H_2-O_2 COMBUSTION

The purpose of this study (Ref. 11) was to produce curves showing the effects of Oxidizer - Fuel Ratio (O/F) and chamber pressure (P_c) on the

steady-state parameters of temperature, specific heat ratio (γ), molecular

weight and charactersitic velocity (C*) in the combustion chamber of an

Impulse Base Flow Facility (IBFF) model. The curves presented in Ref. 11

are intended to provide the engineer with a rapid method for predicting

combustion chamber conditions for gaseous fueled hydrogen-oxygen engines.

4.3   IMPULSE MODEL TEST PROGRAM

References 9 and 10 present the test plan developed to obtain parametric

experimental design data for impulse operated models and tank wave data.

Specific test objectives which were accomplished are:

1. Evaluation of model performance with different:

   ● Combustor volumes (L* = 10,15,25,40 in)
   ● Injector configurations (Triplet, doublet, concentric)
   ● Charge tube pressures
   ● Diaphragm effects (with or without)
   ● Glow plug effects (with or without).

2. Determine the behavior of the blast wave and plume interference
    effects in the vacuum tank for variations in:

   ● Tank pressure
   ● Location in the tank

Figure 8 presents a schematic of an impulse model installed in the tank

bulkhead of the IBFF. The facility basically consists of two charge tubes

(oxidizer and fuel) each containing a flow metering venturi, a diaphragm and

cutter assembly, an injector, a combustion chamber, a nozzle or nozzles and

an altitude simulation chamber. Figure 9 presents an assembly drawing of one

of the configurations tested. The triplet element injector used in these

tests is shown as part of the assembly drawing. The other injectors used

are shown in Figs. 10 and 11. By replacing anular sections of the combustion

chamber (see Fig. 9) the combustor L* was changed allowing four combustor

28

volumes to be tested. The actual volumes and areas for the configurations
tested are listed in Table 11.

A detailed description of the test conducted and results obtained is
given in Refs. 12 and 13. Reference 13 documents the test program with
respect to the impulse model characteristics and Reference 12 documents the
tank wave data. Reference 13 also gives a detailed discussion of model de-
sign methods. Each major component of an impulse operated model is dis-
cussed in terms of previous designs and recommended design methods. The
components considered are charge tube, venturi, diaphragm cutters, diaphragms,
injectors and combustors.

In order to explain the data obtained through this test program and to
provide a design tool for future work, an analytical time dependent combustor
model was developed. Several simplifying assumptions were made to obtain a
tractable model. The basic assumptions consisted of:

1. One dimensional flow
2. Constant combustor specific heat ratio
3. Instantaneous heat release in the combustion chamber by the
   products present
4. Temperature independent heat release
5. Instantaneous perfect mixing within the combustion chamber
6. Constant temperature throughout the manifolds
7. Combustion chamber species were limited to H_2, O_2 and H_2O
8. The nozzle throat diaphragm opens instantaneously at a specified
   pressure.

Based on these assumptions, a time dependent math model for the transient
behavior of the combustor was derived by writing mass, pressure, and energy
balances.

Balance equations were written for:

1. H_2 mass balance in the volume preceding the injector face (H_2 mani-
   fold volume)
2. O_2 mass balance in the volume preceding the injector face (O_2 mani-
   fold volume)

3. Pressure balance across H_2 and O_2 injector ports
4. Combustion chamber mass balance
5. Combustion chamber energy balance
6. Combustion chamber species balance for H_2, O_2 and H_2O.

The mathematical form of these balances are given in Table 12 along with

other equations required for complete definition of the combustor processes.

A few comments are relevant to the equations given in Table 12. The

injector pressure loss equations specify the velocity through the injector

ports leading to the combustion chamber. Choked flow through the ports was

assumed until the chamber pressure rose to 52.8 percent of the respective

manifold pressures. The energy balance equation was derived by specifying

all input, output, and accumulation terms. The relation given by Eq. 8 was

then obtained by subtracting $\overline{C}_p(T - 1080)$ times Eq. 7 from the original equa-

tion. The effects of variable O/F on $\overline{C}_p$ have been included by including a

multiple segment interpolation calculation of $\overline{C}_p$ as a function of O/F.

In order to compare the results from the transient equation to steady

state conditions, the steady state equations for the combustor were derived.

The equations are given in Table 13 and consist of basically the same type

as given in Table 12.

The set of coupled time dependent equations given in Table 12 were

solved numerically using a simple Euler's numerical integration method.

This method was found to be satisfactory if sufficiently small step size

was used. In all cases considered the transient solution obtained the steady

state value if the integration was extended over a sufficient time interval.

A complete documentation of the computer code for the solution of the

steady and transient equations is given in Ref. 13.

The transient math model has been used to analyze the data obtained

during the test program. Fig. 12 presents a comparison of the theoretical transient response of the three main configurations studied experimentally. It can be noted that the doublet injector configuration obtained steady state more quickly than the other configurations. This was verified experimentally. Figure 13 shows a comparison of the theoretical method with data. The comparison is quite satisfactory for design work and is typical of the many cases studied in Ref. 13.

Reference 12 presents the measurements made in the altitude simulation chamber or vacuum tank to determine the effects of the reflected blast wave on the nozzle exhaust plume for variations in tank pressure and tank location. The prime objective of the vacuum tank measurements was to determine the time interval for which steady state conditions existed in the exhaust flow before the reflected wave disturbed the flow. A secondary objective was to attempt photographic coverage of the plume during steady state conditions. To accomplish this objective color and infrared film were used and the f-stop setting and development procedure were varied. Only marginal success was achieved.

The reduced data presented in Ref. 12 for the primary test objective consists of different tables and plots of the time at which the initial and reflected waves passed different probe positions. These plots were then used to construct a graphic representaiton of the wave patterns which existed at different time intervals after firing the model. The data was compiled for the three test altitudes, i.e. 240 Kft., 280 Kft., and 320 Kft. All the wave data at a given altitude was averaged together and no distinction was made for different L*, injector arrangements or diaphragm burst pressures.

The wave patterns given in Figs. 14 to 19 show the initial and reflected wave at different times for each of the three test altitudes, 240, 280, and 320 Kft. For each altitude the initial wave is shown at times 0.5, 1.0, 1.5, and 2.0 millisec. and the reflected wave is shown at times of 5.0, 7.5, 10.0. and 15.0 millisec. For the initial wave patterns constructed, the following items were noted.

1. As the test altitude was increased the initial wave exhibited an expected broadening due to the expansion into a lower pressure.

2. Likewise as the altitude increased the wave speed increased. At 240 Kft. the wave was just reaching the tank end and side wall at 2.5 millisec. while at the 320 Kft the wave had almost reached the side wall at 1.5 millisec.

3. The shape of the wave also changed with increasing altitude. At the lower altitudes the wave front had a parabolic shape that changed to a wave front which was almost perpendicular to the tank centerline at 320 Kft. At each altitude the wave was found to be relatively flat and parallel with the nozzle exit for some distance from the exit. It appeared that this flatness was maintained for a longer time at the higher altitudes.

4. The waves in the region which is shown in the figures as extending from the lip of the nozzle toward the tank wall were found to move slowly in comparison to that movement in the frontal wave regions. In fact, there was strong evidence to support an argument that the phenomena observed was not that of a wave but simply the gas front expansion. This argument was supported by the fact that the phe-

nomena in most of this region was moving at a speed that was less

than Mach 1 and that the thin film gauge responses did not exhibit

the rather abrupt change associated with a strong blast wave. The

movement in the region was so slow that the reflected wave from the

tank side wall appeared to overtake the initial gas expansion.

The reflected wave patterns are of even greater significance to short

duration rocket motor tests at simulated altitudes because the arrival of the

reflected wave within the plume or model base region destroys the altitude

simulation and signifies the end of the test time. It was unfortunate then

that the reflected wave patterns were more difficult to establish and identify

than the initial wave. This was because at the time of the passage of the

reflected wave, the thin film gauge was still responding to the passage of

the initial wave and the gas following it. Although this in itself made

the identification of the passage of the second wave difficult, in addition,

the reflected wave was weaker than the initial wave and therefore did not

produce a pronounced change in the gauge response. For these reasons the

reflected wave data was found to be more scattered than the initial wave

data. For the reflected wave patterns constructed, the following items were

noted.

1. The reflected wave and/or gas movement region which was likely to

   first cause steady flow breakdown was found to occur from the tank

   side walls and to form a "U" shaped pattern which generally moved

   along the plume boundary.

2. Although the reflected wave movement pattern differed somewhat

   with altitude, it was found to arrive within the nozzle base region

   at approximately the same time. Average arrival times at the tank

bucket corner were 11.8, 11.0, and 9.8 msec for 240, 280, and

320 Kft. altitudes respectively.

3. As noted earlier in the discussion of the initial wave, the region

    from the nozzle lip to the tank side wall has a very weak initial

    wave and is probably only the gas expansion in that region. For

    this reason it is likely that no well defined reflected wave comes

    directly off the side wall. The sketched reflected wave patterns

    are most likely a combination of wave phenomena and gas front ex-

    pansion. The "U" shaped wave, even though it is produced within

    a region where the reflected wave is very weak, moves rapidly back

    to the nozzle region because it has very little or no gas velocity

    head to move against, thereby achieving a rather quick relative

    movement.

4. There was some evidence of the existence of a third wave phenomena.

    However, the data obtained were inconclusive, so no definition of

    its wave pattern was made. This wave was suspected to come from the

    region where the tank far end wall joins the tank side wall. The

    wave movement would be along the tank side wall and behind the wave

    reflected from the tank side wall.

	12 Element Triplet		6 Element Triplet		Concentric		Doublet	
	O_2	H_2	O_2	H_2	O_2	H_2	O_2	H_2
Venturi Diffuser + Diaphragm Bulge Volume (in.^{3})	0.951	0.914	0.951	0.914	0.951	0.914	0.951	0.914
Injector Housing – Diaphragm Bulge Volume (in.^{3})	0.474	1.150	0.474	1.150	0.474	1.150	0.474	1.150
Injector Volume (in.^{3})	1.958	4.493	1.542	4.493	2.603	8.253	0.621	3.054
Total (in.^{3})	2.432	5.643	2.016	5.643	3.077	9.403	1.095	4.204
Injector Face Element Area (in.^{2})	0.782	0.372	0.391	0.186	0.964	1.374	0.230	0.230
Combustion Volume in Injector (in.^{3})	2.946		2.946		2.936		6.193	
	Vol. to Diaph.	Throat	Vol. to Diaph.	Throat	Vol. to Diaph.	Throat	Vol. to Diaph.	Throat
Nozzle and Adapter	3.54	6.12	3.54	6.12	3.54	6.12	3.54	6.12
Nominal L* = 10 Comb. Section	4.47	4.47	4.47	4.47	4.47	4.47	4.47	4.47
Total for L* = 10	10.96	13.54	10.96	13.54	10.95	13.53	14.20	16.78
Actual L* (in.) for L* = 10#	12.4		12.4		12.4		15.4	
Nominal L* = 15 Comb. Section	9.84	9.84	9.84	9.84	9.84	9.84	9.84	9.84
Total for L* = 15	16.33	18.91	16.33	18.91	16.32	18.90	19.57	22.15
Actual L* (in.) for L* = 15	17.3		17.3		17.3		20.3	
Nominal L* = 25 Comb. Section	20.83	20.83	20.83	20.83	20.83	20.83	20.83	20.83
Total for L* = 25	27.32	29.90	27.32	29.90	27.31	29.89	30.56	33.14
Actual L* (in.) for L* = 25	27.4		27.4		27.4		30.4	
Nominal L* = 40 Comb. Section	37.20	37.20	37.20	37.20	37.20	37.20	37.20	37.20
Total for L* = 40	43.69	46.27	43.69	46.27	43.68	46.26	46.93	49.51
Actual L* (in.) for L* = 40	42.5		42.5		42.4		45.4	

A* = 1.091 in.^{2}

TABLE 12

TRANSIENT EQUATIONS FOR GASEOUS PROPELLANT
IMPULSE OPERATED COMBUSTORS

O_2 - Manifold Mass Balance

$$V_0 \frac{d\rho_0}{dt} = m_0 - \rho_0 U_0 A_0 \tag{1}$$

H_2 - Manifold Mass Balance

$$V_H \frac{d\rho_H}{dt} = m_H - \rho_H U_H A_H \tag{2}$$

O_2 - Injector Pressure Loss

$$P_c = P_0 - \rho_0 U_0^2 F_0 / g_c \tag{3}$$

$$U_0 = C_0 \text{ if } P_c/P_0 < 0.528$$

H_2 - Injector Pressure Loss

$$P_c = P_H - \rho_H U_H^2 F_H / g_c \tag{4}$$

$$U_H = C_H \text{ if } P_c/P_H < 0.528$$

Equation of State

$$P = \rho RT/M \tag{5}$$

Speed of Sound

$$C = (\gamma RT g_c/M)^{1/2} \tag{6}$$

TABLE 12 (Cont. 1)

Combustor Mass Balance

$$V_c \frac{d\rho_C}{dt} = (\rho UA)_0 + (\rho UA)_H - \rho_c K C_c A^* D \qquad (7)$$

where

D = 0 Before the nozzle diaphragm burst

= 1 After the nozzle diaphragm burst

$$K = \left(\frac{2}{\gamma+1}\right)^{(\gamma+1)/2(\gamma-1)} \qquad \gamma = 1.135 \text{ assumed for O/F} = 6.0$$

Combustor Energy Balance

$$\rho_c V_c C_p \frac{dT}{dt} = \left(Hr_W - \left[(\rho UA)_H + (\rho UA)_0\right] \bar{C}_p (T-1080)\right.$$

$$\left. -126(\rho UA)_0 - 1903(\rho UA)_H + \frac{V_c}{J}\frac{dP}{dt}\right) \qquad (8)$$

where H = heat of reaction (5730 Btu/lbm of H_2O)

Combustor Species Balance

O_2 - Balance

$$\frac{dW_O}{dt} = (\rho UA)_0 - \frac{W_O}{W_T} \rho_c A^* C_c KD - r_O \qquad (9)$$

where

$$r_O = (\rho UA)_0 \text{ if } W_O/W_H \leq 8$$

$$= \frac{8}{9}\frac{dW_W}{dt} \text{ if } W_O/W_H > 8$$

H_2 - Balance

$$\frac{dW_H}{dt} = (\rho UA)_H - \frac{W_H}{W_T} \rho_c A^* C_c KD - r_H \qquad (10)$$

TABLE 12 (Cont. 2)

where

$$r_H = (\rho UA)_H \quad \text{if } W_O/W_H > 8$$

$$= \frac{1}{9} \frac{dW_W}{dt} \quad \text{if } W_O/W_H \leq 8$$

H_2O - Balance

$$\frac{dW_W}{dt} = r_W - \frac{W_W}{W_T} \rho_C A^* C_C KD \tag{11}$$

where

$$r_W = \frac{9}{8} \frac{dW_O}{dt} \quad \text{if } W_O/W_H \leq 8$$

$$= 9 \frac{dW_H}{dt} \quad \text{if } W_O/W_H > 8$$

Combustor Mass

$$W_T = W_H + W_O + W_W \tag{12}$$

Combustor OF

$$(OF)_C = (W_O + 8W_W/9)/(W_H + W_W/9) \tag{13}$$

Combustor Molecular Weight

$$M_C = (W_H + W_W)/(W_H/2 + W_W/18) \quad \text{if } W_O/W_H \leq 8 \tag{14}$$

$$M_C = (W_O + W_W)/(W_O/32 + W_W/18) \quad \text{if } W_O/W_H > 8 \tag{15}$$

TABLE 13

STEADY STATE EQUATIONS FOR GASEOUS PROPELLANT
IMPULSE OPERATED COMBUSTORS

___

Combustor OF

$$(OF)_c = m_0/m_H \tag{1}$$

Combustor Molecular Weight

$$M_c = 2(OF)_c + 2 \quad \text{if } (OF)_c \leq 8 \tag{2}$$

$$M_c = 32((OF)_c + 1)/((OF)_c + 8) \quad \text{if } (OF)_c > 8 \tag{3}$$

Combustor Species

Before combustion (mass ratios)

$$W_0/W_T = (OF)_c/((OF)_c + 1) \tag{5}$$

$$W_H/W_T = 1 - W_0/W_T \tag{6}$$

Before combustion (mole to mass ratios)

$$N_H/W_T = \frac{1}{2} W_H/W_T \tag{7}$$

$$N_0/W_T = \frac{1}{32} W_0/W_T \tag{8}$$

Post combustion (mole to mass ratio of H_2O)

$$N_W/W_T = 2 N_0/W_T \quad \text{if } (OF)_c \leq 8 \tag{9}$$

$$= N_0/W_T \quad \text{if } (OF)_c > 8 \tag{10}$$

TABLE 13 (Cont. 1)

Post combustion (mass ratio)

$$W_w/W_T = 18 \, N_w/W_T \tag{11}$$

Combustor Energy

$$T = H(W_w/W_T)/C_p \tag{12}$$

Speed of Sound

$$C_c = (\gamma_c RT g_c/M_c) \tag{13}$$

Combustor Mass Balance

$$\rho_c = (m_o + m_H)/(KC_cA^*) \tag{14}$$

$$\text{where} \quad K = \left(\frac{2}{\gamma+1}\right)^{(\gamma+1)/2(\gamma-1)}$$

Combustor Pressure

$$P_c = \rho_c RT/M_c \tag{15}$$

Injector Face Densities

$$\rho_{oc} = P_c M_o/RT_o \tag{16}$$

$$\rho_{Hc} = P_c M_H/RT_H \tag{17}$$

Injector Velocities

$$U_o = m_o/(A_o \rho_{oc}) \tag{18}$$

$$U_H = m_H/(A_H \rho_{Hc}) \tag{19}$$

TABLE 13 (Cont. 2)

Injector Pressures

$$P_o = P_c + \rho_{oc} \, U_o^2 \, F_o/g_c \tag{20}$$
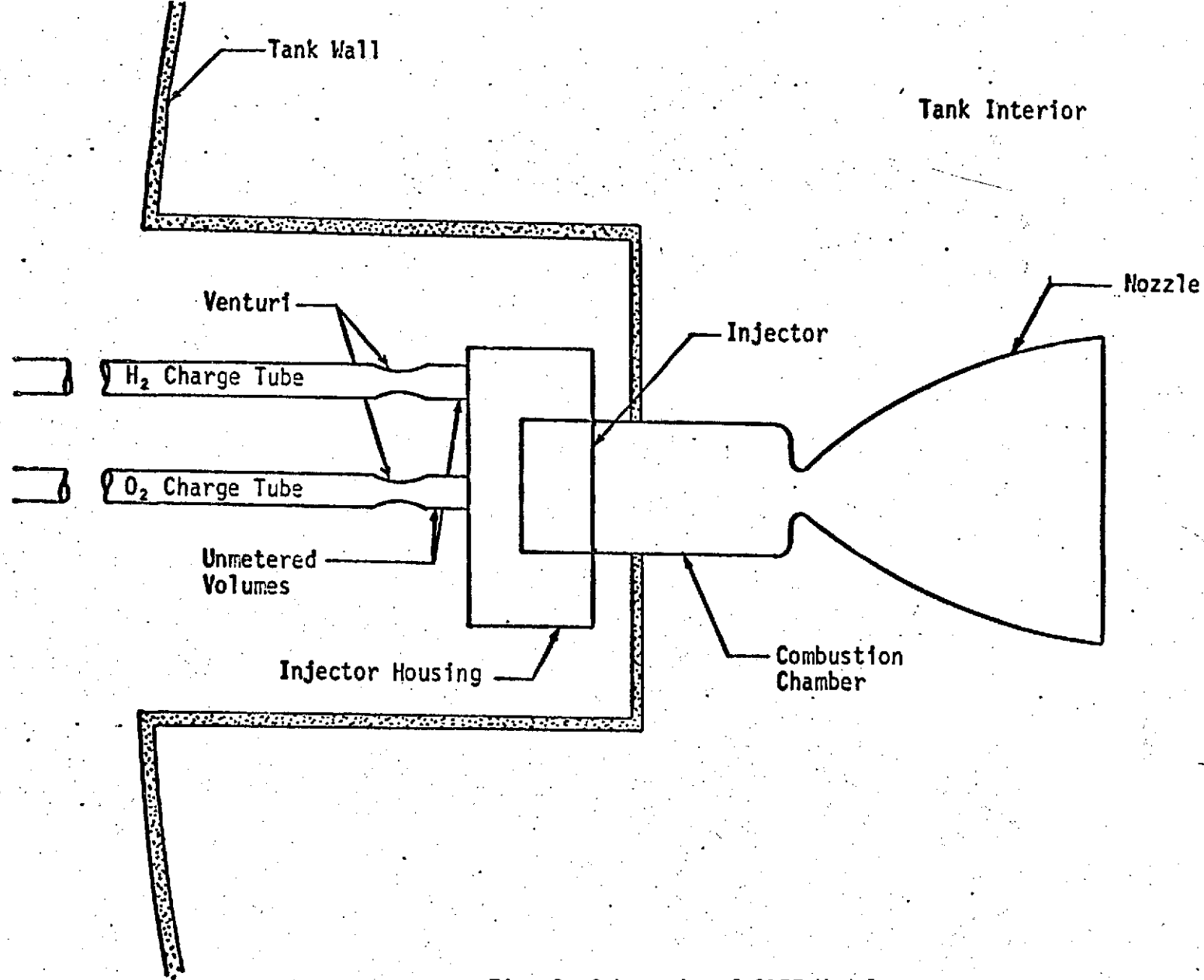
$$P_H = P_c + \rho_{Hc} \, U_H^2 \, F_H/g_c \tag{21}$$
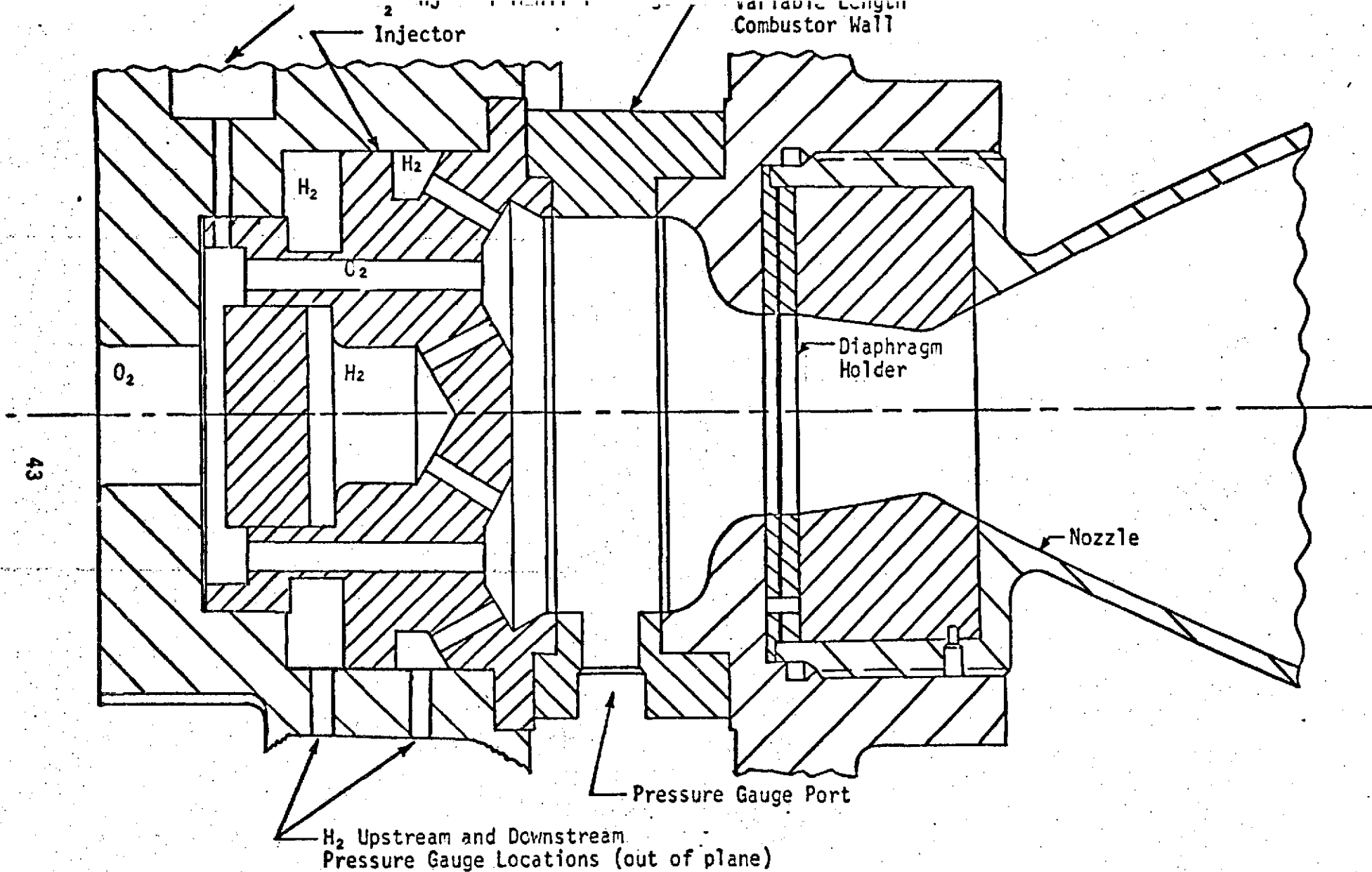
Fig. 8   Schematic of IBFF Model

Injector

H_2

Variable Length
Combustor Wall

H_2

H_2

O_2

H_2

O_2

Diaphragm
Holder

Nozzle

Pressure Gauge Port

H_2 Upstream and Downstream
Pressure Gauge Locations (out of plane)

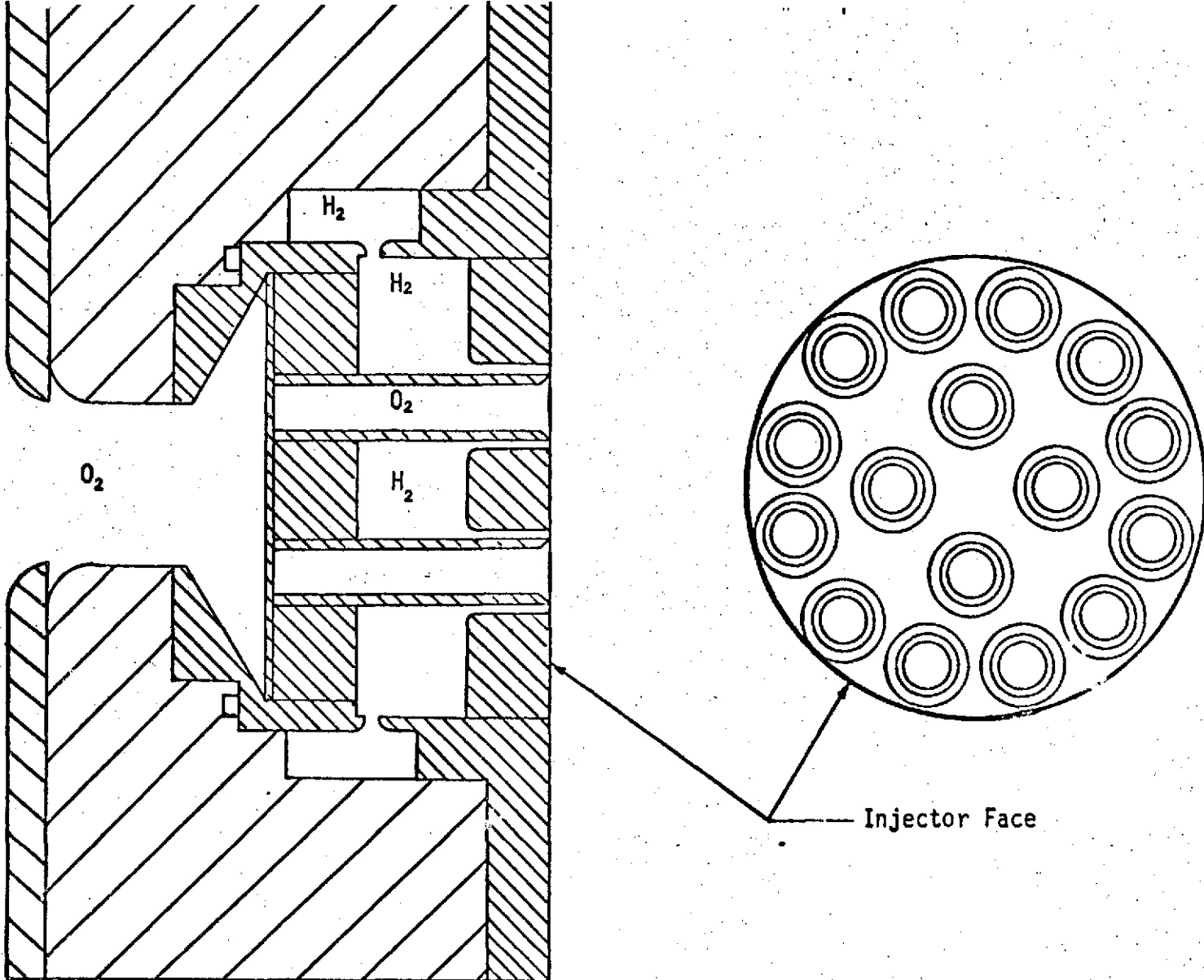Fig. 9 Combustor Assembly, L* = 10 in., Triplet Injector

44
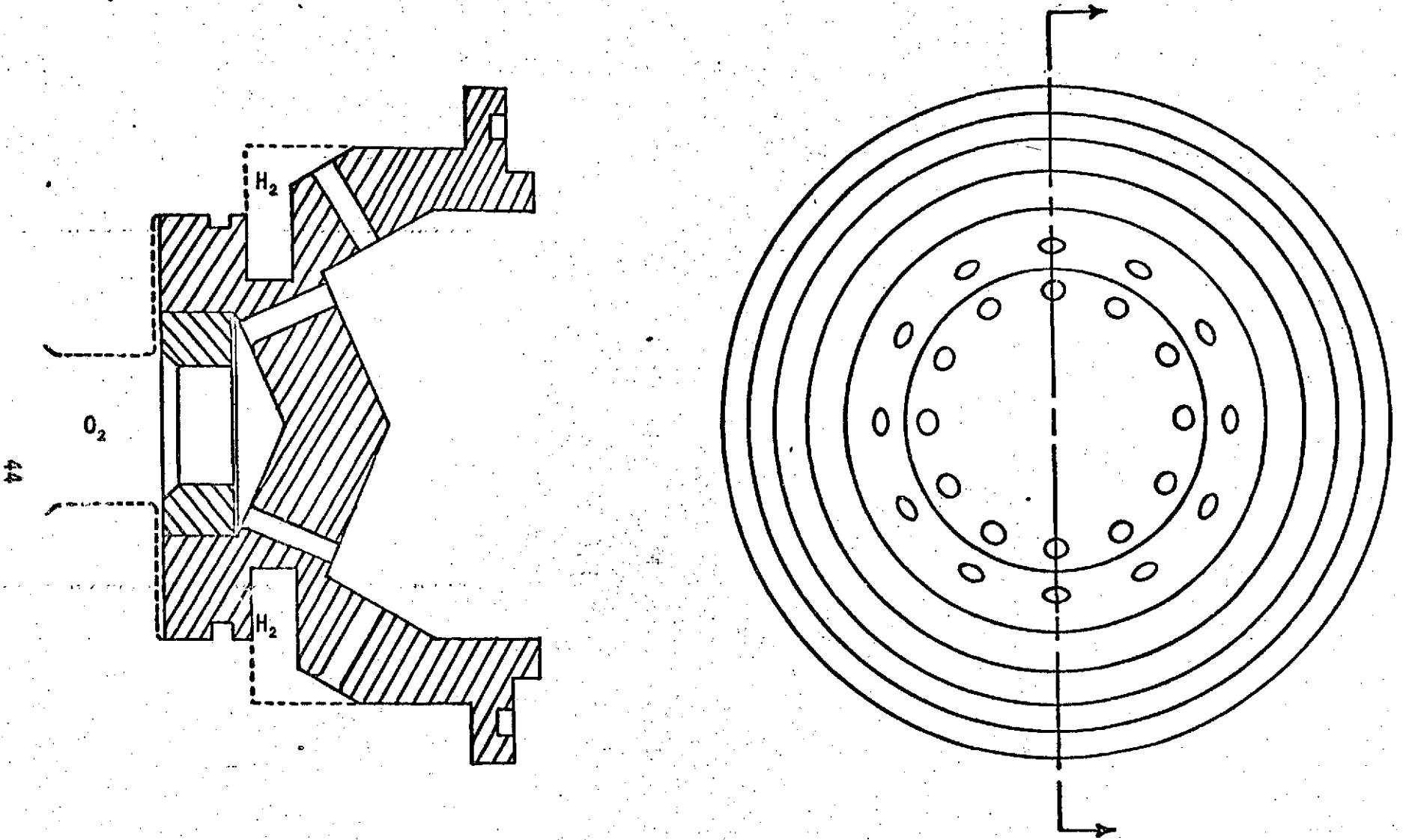
Fig. 10   Doublet Element Injector Geometry

Fig. 11   Concentric Orifice Injector
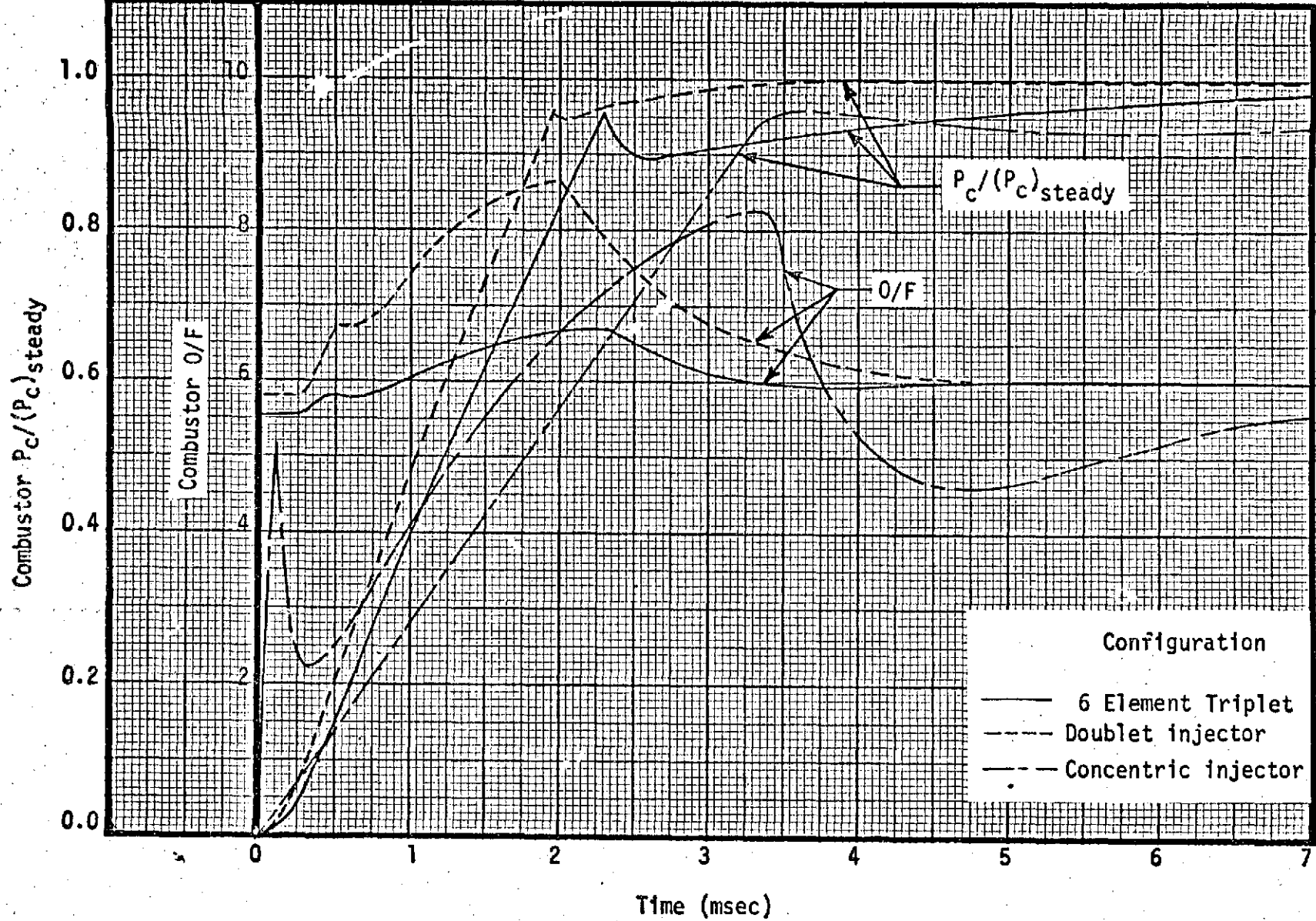
Fig. 12 Theoretical Start-up Processes of 8% J-2 Combustor with the Doublet and Triplet and Concentric Injectors for L* = 25 and $P_{CB}/(P_C)_{steady}$ = 0.956
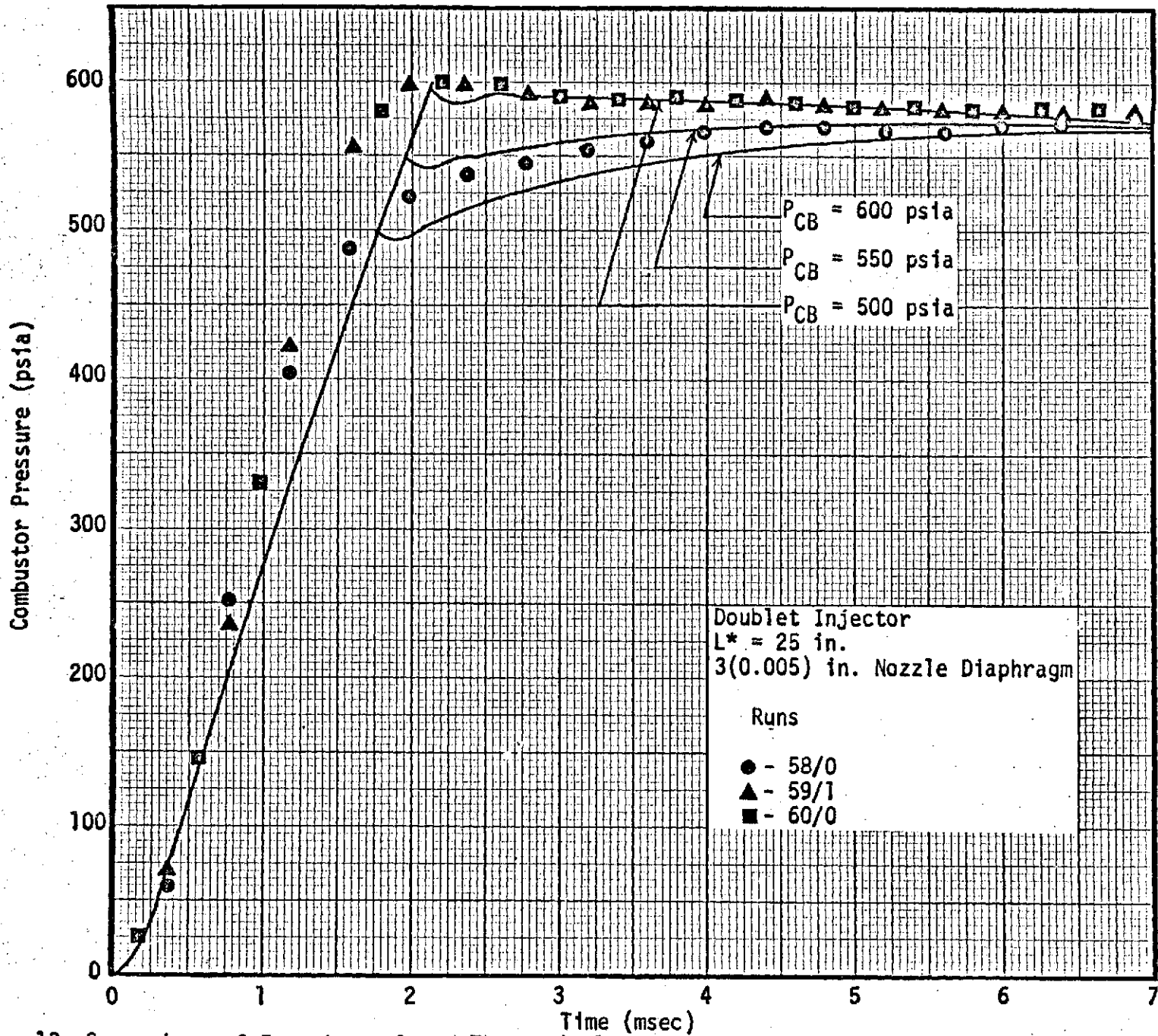
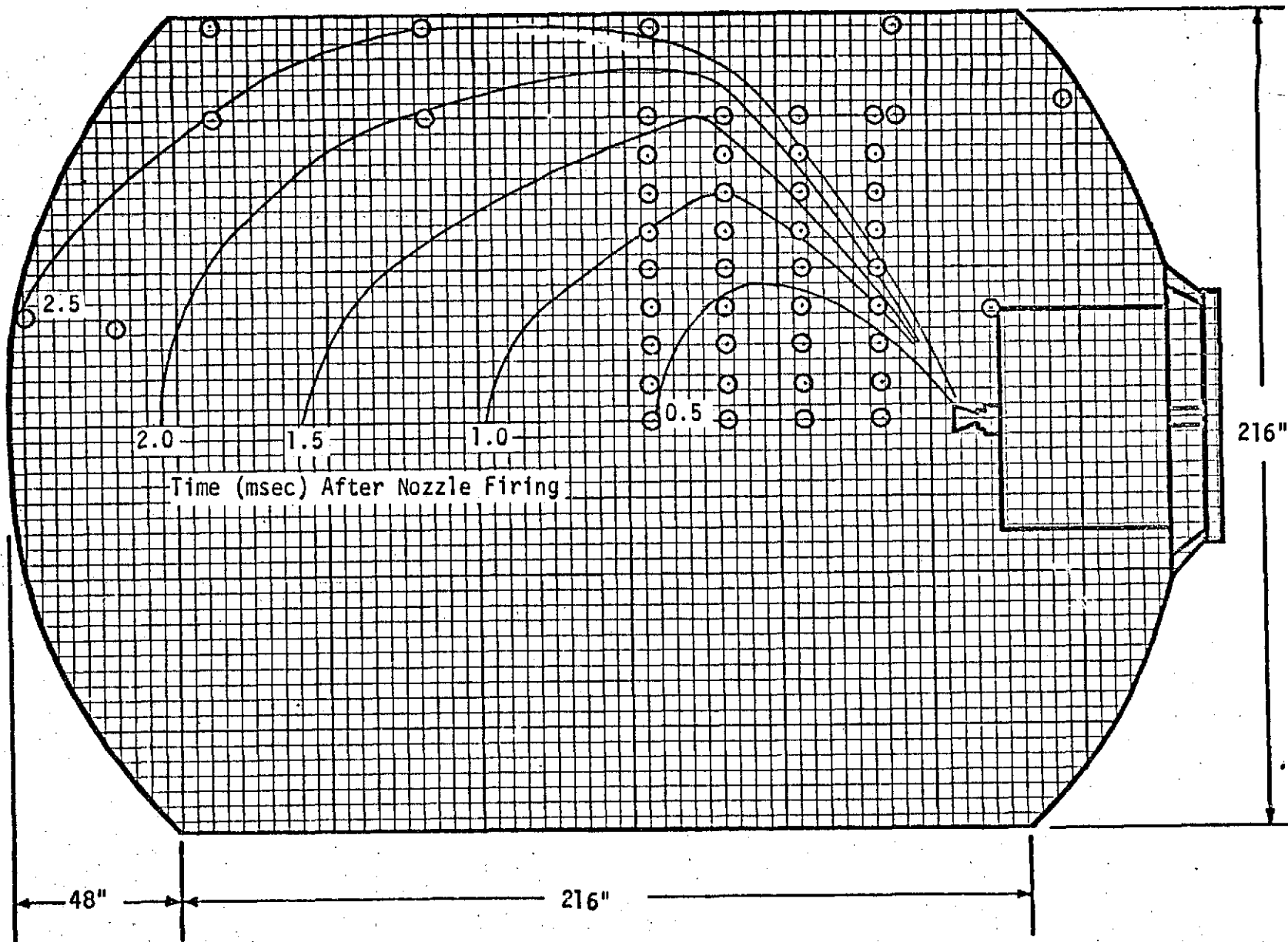Fig. 13 Comparison of Experimental and Theoretical Combustor Pressure Histories for the Doublet Injector

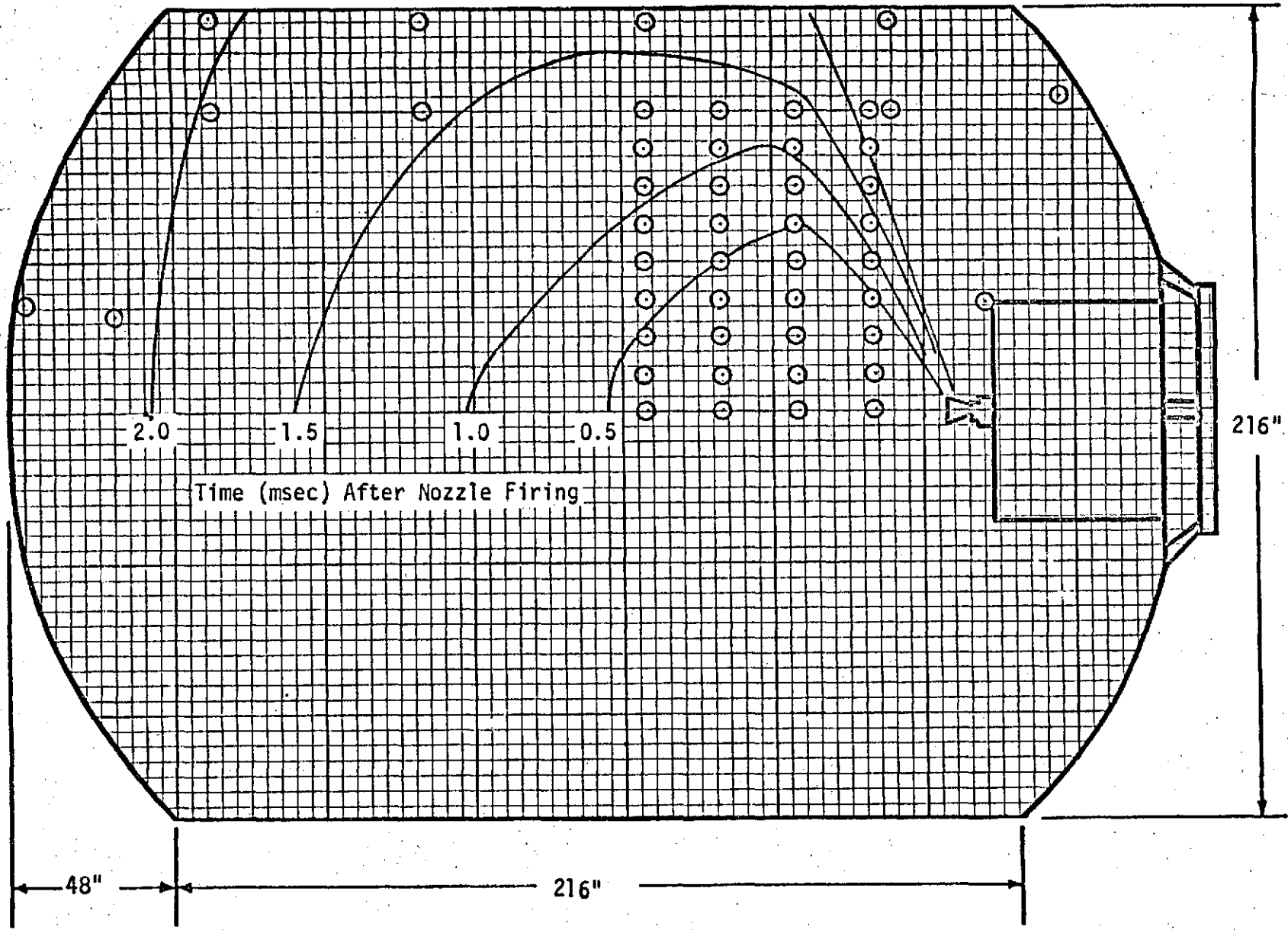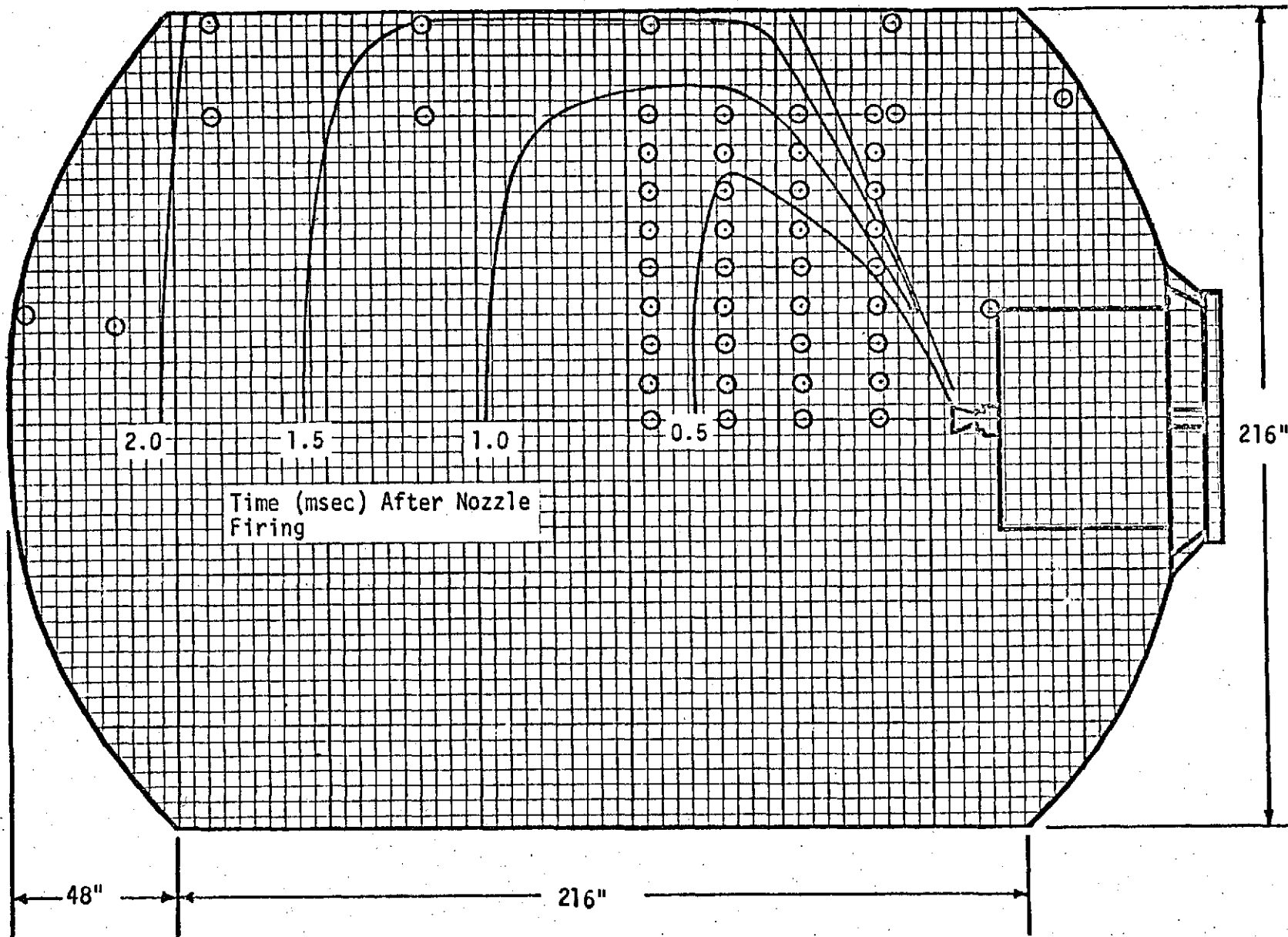Fig. 14 Tank Initial Wave Contours at Simulated Altitude of 240 Kft.

Fig. 15 Tank Initial Wave Contours at Simulated Altitude of 280 Kft.

Fig. 16   Tank Initial Wave Contours at Simulated Altitude of 320 Kft.

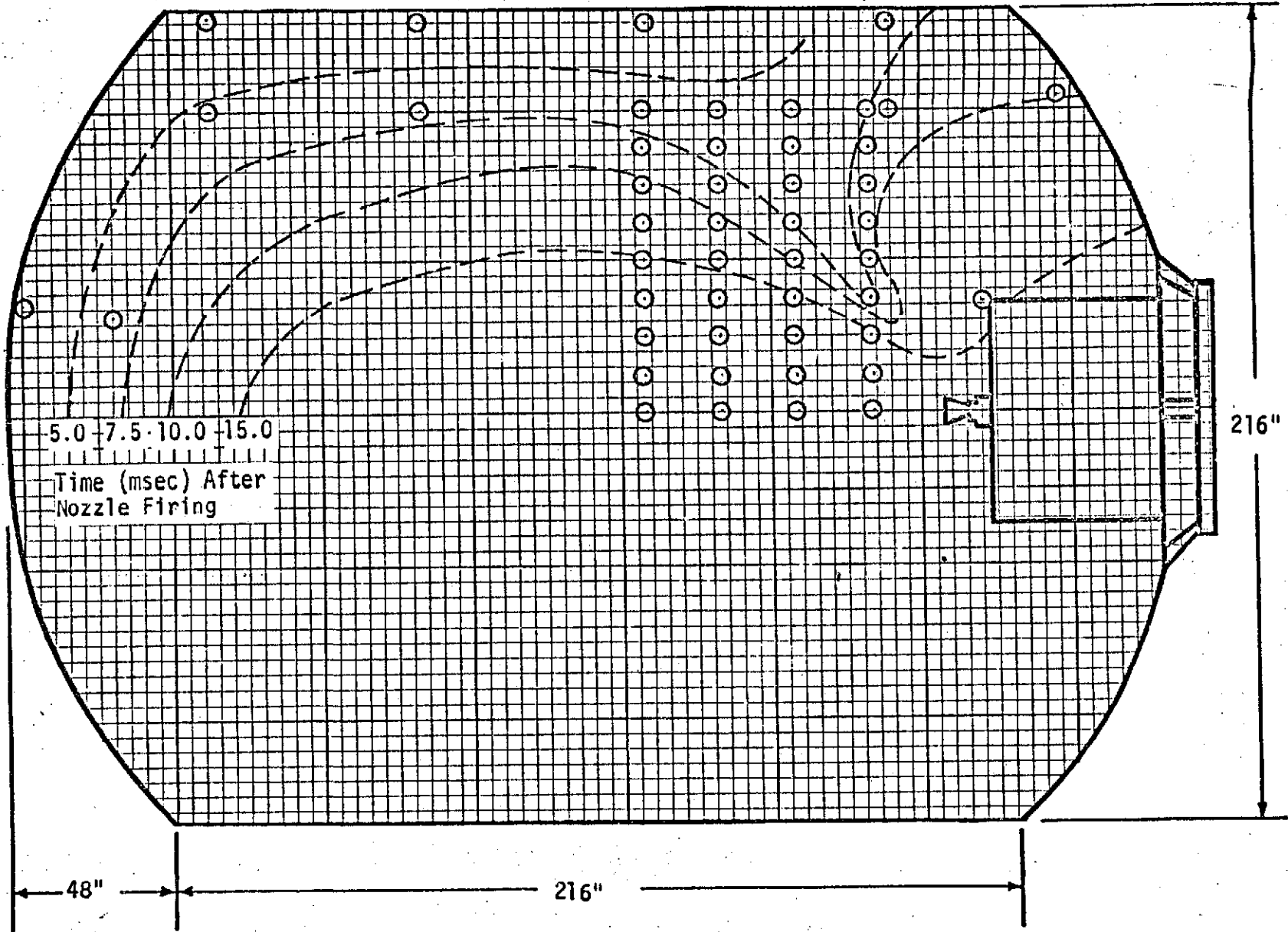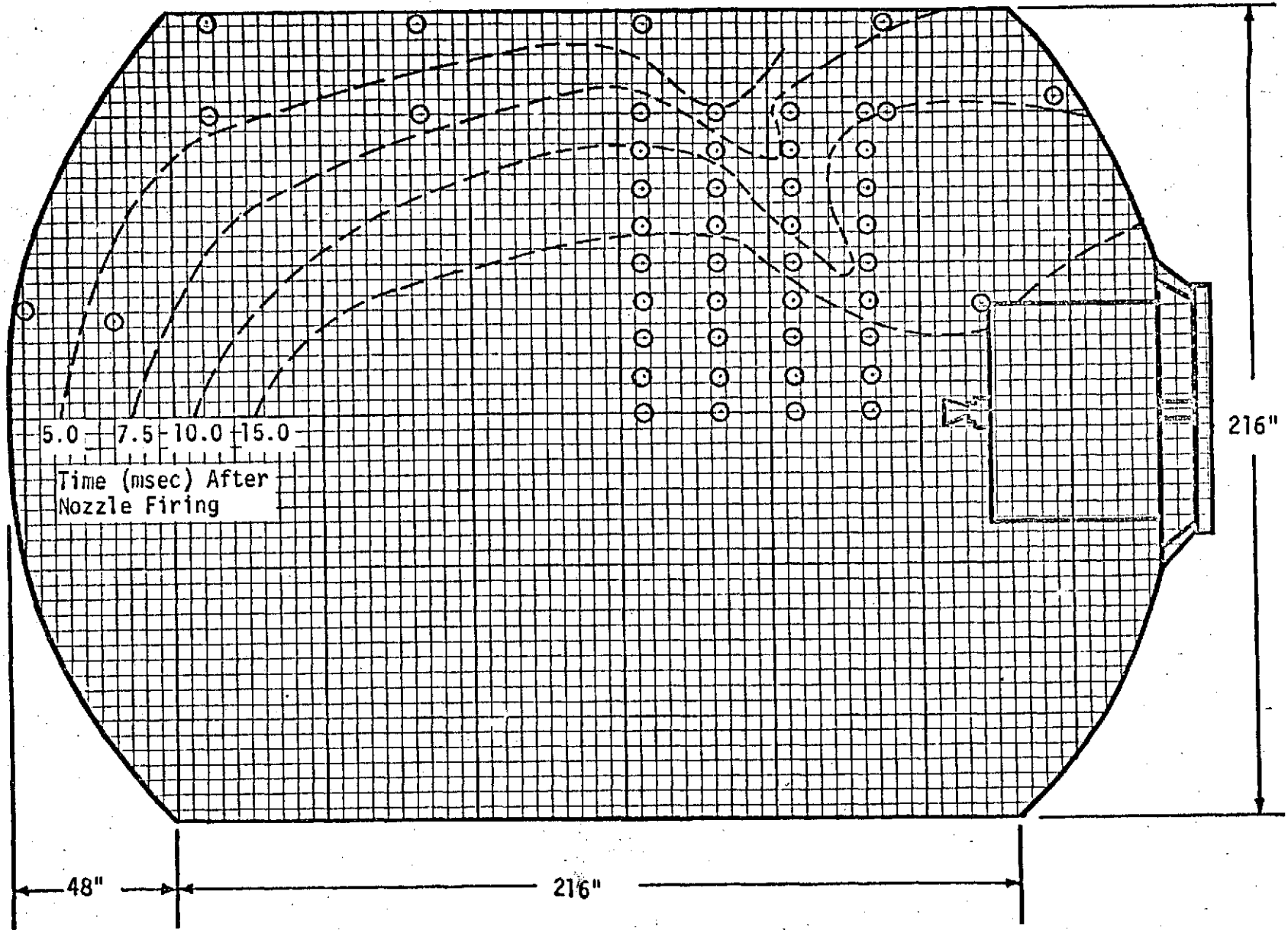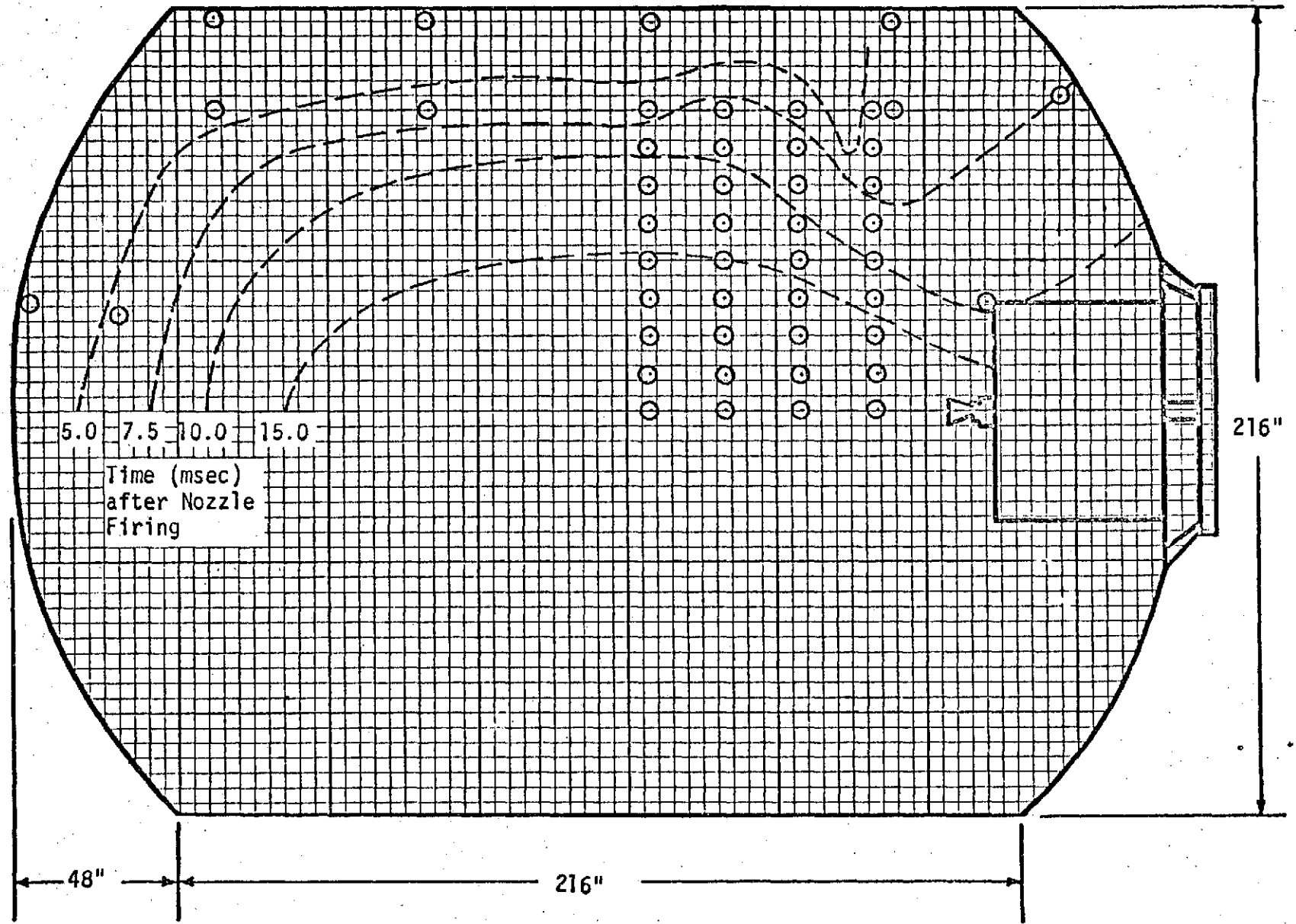Fig. 17 Tank Reflected Wave Contours at Simulated Altitude of 240 Kft.

Fig. 18   Tank Reflected Wave Contours at Simulated Altitude of 280 Kft.

Fig. 19 Tank Reflected Wave Contours at Simulated Altitude of 320 Kft.

Section 5

CONCLUSIONS

The work conducted under this contract included several technical areas. These areas have been summarized in the preceding section and fall within the following groupings.

1. Cavity Heating (Ref. 1 and 2)

2. Rarefied Flow Heating (Ref. 3 to 7)

3. Impulse Model Research (8 to 13)

Specific documentation has been given in each of these groupings as indicated by the noted references. In each of the three groupings either methodology improvements were achieved or experimental data has been obtained which provides a more complete understanding of the areas studied.

Section 6

REFERENCES

1. Engel, Carl D., "The Propulsive Attitude Control System - An Open
    Cavity Heating Problem," REMTECH, Inc., RTR 008-1, April 1972.

2. Engel, Carl D., "Synopsis for Thermal Environment Predictions of
    Two Cavity Regions of External Tank," REMTECH, Inc., RM 008-7,
    February 1973.

3. Engel, Carl D., "Aeroheating Correlations for Noncontinuum Hypersonic
    Flight," REMTECH, Inc., RTR 008-2, December 1972.

4. Engel, Carl D., "Saturn 501, Rarefied Flow Heating Data Review,"
    REMTECH, Inc., RM 008-9, June 1973.

5. Engel, Carl D., "A Simple Recovery Enthalpy Relation for Hypersonic
    Flight," REMTECH, Inc., RM 008-6, January 1973.

6. Engel, Carl D., "Modifications for Noncontinuum Aeroheating Calcula-
    tions to the MINIVER Program," REMTECH, Inc., RM 008-5, February 1973.

7. Engel, Carl D., "MINIVER Computer Program Listing with Rarefied Flow
    Aeroheating Modifications," REMTECH, Inc., RM 008-8, April 1973.

8. Engel, Carl D., "An Investigation of Impulse Base Flow Facility Data,"
    REMTECH, Inc., RM 008-3, August, 1972.

9. Engel, Carl D. and Reardon, John E., "IBFF Model Research Program Pre-
    test Report", REMTECH, Inc., RM 008-2, June 1972.

10. Reardon, John E. And Engel, Carl D., "IBFF Model Research Program Pre-
    test Report (Modified)," REMTECH, Inc., RM 008-2A, January 1973.

11. Somers, Richard E. and Engel, Carl D., "Chamber Properties of Gaseous
    Oxygen-Hydrogen Combustors," REMTECH, Inc., RM 008-10, August 1973.

12. Fuller, Charles E. and Engel, Carl D., "IBFF Vacuum Tank and Blast
    Wave Data Report," REMTECH, Inc., RM 008-4, May 1974.

13. Reardon, John E. and Engel, Carl D., "IBFF Combustor Design and Data
    Analysis," REMTECH, Inc., RTR 008-3, May 1974.

14. Burggraf, Odus R., "A Model of Steady Separated Flow in Rectangular
    Cavities at High Reynolds Number," Proceedings of the 1965 Heat Transfer
    and Fluid Mechanics Institute, Andrew F. Charwat, ed., Stanford Univer-
    sity Press, 1965, pp. 190-229.

15. Hodgson, J. W., "Heat Transfer in Separated Laminar Hypersonic Flow,"
    AIAA J., Vol. 8, No. 12, December 1970.

REFERENCES (Con't)

16. Denison, M. R., and E. Baum, "Compressible Free Shear Layers with Finite Initial Thickness," <u>AIAA J.</u>, Vol. 1(2), 1963, p. 342.

17. Oppenheim, A. K., "Generalized Theory of Convective Heat Transfer in a Free-Molecule Flow," <u>J. Aeron. Sci.</u>, Jan. 1963, p. 49.

18. Shorenstein, M. L., and Probstein, R. F., "The Hypersonic Leading-Edge Problem," <u>AIAA J.</u>, Vol. 6, No. 10, Oct. 1968.